國立臺灣大學工學院應用力學研究所

碩士論文

Graduate Institute of Applied Mechanics
College of Engineering
National Taiwan University

Master Thesis

雙電極石英晶體微天平共振之提昇能量集中的三維數值模擬

Three Dimensional Simulations of Enhancing Energy Concentration for a Dual-channel Quartz Crystal Microbalance Thickwise Shear Resonance

廖銘威

Ming-Wei Liao

指導教授：張正憲 博士
趙聖德 博士

Advisor: Jeng-Shian Chang, Ph. D.
Sheng-Der Chao,Ph. D

中華民國 九十八 年 七 月

July, 2009

摘要

隨著檢測要求的提升及製程技術的純熟，多通道石英晶體微天秤不僅成為可行的夢想，更是未來生物感測器的發展目標

在此論文裡，首先考慮了二維模型模擬。在此，我們利用了以往的研究中，已經證明的平台式設計來提升 QCM 的敏感度及準確性，然而在某些特定的設計尺寸下，其 QCM 的能量井效應會有大幅減少的現象，當此現象發生時會使得量測工作準確度下降。接著，在考慮了二維問題時的平面應力下,當展成三維模型時，我們將其展成三種不同的形式，並且討論各平台的高度對於能量井效應的變化，但由結果中仍然發現其掉落現象的發生。因此我們再引進了步階式的設計，並且希望能夠改進此現象。而本文的目標則是為了將 QCM 的設計最佳化，也因此在本文的最後會經由模擬結果，建議往後 QCM 適當的設計模型及相關的尺寸。

關鍵字：雙通道石英晶體微天平、壓電材料、平台設計、步階設計，能量井效應、有限元素法

Abstract

With the increasing need for gauge and the substantial progress of wafer fabrication technique, Multi-channel Quartz Crystal Microbalance (MQCM) is very attractive for biosensor applications.

In this paper, 2D simulations are performed first. The mesa-design dual-channel QCM is utilized to improve the sensitivity and stability. However, the energy trapping effect will decrease suddenly under some specific geometry. This phenomenon is called dropping effect, and those specific sizes are called dropping points. Then, under the assumption of 2D plane strain problems, three distinct 3D mesa-design models are introduced for the simulation. Then, the energy trapping effect varied with mesa height will be discussed for each. Unfortunately, the dropping effect still exists. Therefore, to meliorate the phenomenon, the bi-step design is recommended. Finally, the suggested design dimension and model have been established by the process of optimizing dual-channel quartz crystal microbalance.

Key words: dual-channel quartz crystal microbalance, piezoelectric material, mesa design, bi-step design, energy trapping effect, finite element method

誌謝

首先感謝指導老師 張正憲老師在這兩年中，不論是研究方向、問題解惑等都給予悉心指導，更甚者，對於做事的態度及未來的方向，亦有很大的啟發，使我在這兩年的研所時間裡，所見所聞更加寬廣。在論文口試期間，承蒙指導老師 趙聖德老師與口試評審委員 吳光鐘老師的建議及指正，使得論文不足處得以補強進而更臻完善，在此獻上由衷感謝。

此外感謝在這兩年來陪伴如側的實驗室伙伴們，感謝冠榮總是在我遇到問題時對我伸出援手，以及分享生活中的趣事，來排解做研究時的苦悶。謝謝學長們的幫助，為我解決了課業上的問題和研究上的瓶頸。謝謝同窗的上瑋、之珉、孟謙、美娟、致嘉，有大家一起的奮鬥，才能渡過高壓的研一課業。另外謝謝學弟妹們在我最後一年的研所生涯裡，陪我們聊天談心，注入快樂的活力。謝謝所有229 室的朋友們。

此外，感謝我的家人，謝謝你們對我的如此長時間的疼愛和關心。謝謝我的雙親國基、順招你們的恩情我點滴在心頭。謝謝大姐每次刀子口豆腐心的為我著想。謝謝二姐純芳每次都為我打點在台北的事務。謝謝女友慧敏不離不棄的關心和照顧。並在此特別感謝我的二姐純芳和女友慧敏，沒有你們的幫忙與守護，我的論文不能夠如期完成。真的謝謝你們一直陪伴著我。

僅此以這些短短文字獻給所以關心我和幫忙過我的家人和朋友，謝謝你們。

Table of Contents

國立臺灣大學 人品勤學愛國

List of Figures

List of Tables

Chapter 1 Introduction

1.1 Motivation

Since the invention of QCM (Quartz crystal microbalance), it has been applied to measure slight mass variation extensively. In addition, with the increasing need for gauge and the substantial progress of wafer fabrication technique, multi-channel QCM is developed for multiplex measurement. In recent years, QCM array has become a rather popular research topic. The design of multi-channel QCM can not only reduce costs and testing dosage but also shorten the time for measurement.

In general, the multi-channel QCM is easily influenced by an adjacent electrode and which will further affect the testing result. Relative to it, the miniaturization of the biosensor also plays a crucial role in the testing outcome. As a consequence, how to minimize the distance between electrodes without bringing about negative impacts on the function and accuracy is the crux. If we can boost the energy trapping effect of individual electrode on multi-channel QCM efficiently, it means that the influence between each electrode can diminish to minimum and the electrodes can be regarded as independent, respective ones. The subject of this study is to optimize dual-channel QCM with the advantages mentioned above. And the ultimate goal is to enhance the energy trapping effect by designs of mesa and bi-step and obtain the additional benefits of biosensor miniaturization and accuracy promotion along with it.

1.2 Literature Review

QCM (quartz crystal microbalance) is a sensitive instrument that transforms the mechanical signal into an electric one by means of the quartz crystal piezoelectric effect. Curie brothers [1] discovered the piezoelectric effect, in 1880. When exerting an external force to some specific crystal, they detected the existence of a weak electric current, which was then called the direct piezoelectric effect. Afterward, Lord Rayleigh et al [2] found that the resonance frequency would vary according to the alteration of the mass as well as the cutting types of quartz plate. As a consequence, AT-cut quartz is taken as this thesis topic in order to ascertain more of its incontrovertible facts. The main vibration mode of AT-cut quartz is thickness-shear with a little frequency drift induced by temperature variation. This is why many electronic components operating at high frequency would utilize AT-cut quartz as a vibrator.[3, 4]

In 1951, the piezoelectric plate was simplified from infinite to 2D by Mindlin,et al [5] who made vibration equation with the series expansion method when piezoelectric plate is applied to electric potential. In 1959, Sauerbrey et al [6] perceived that the relation between the resonance frequency drift of quartz crystal thickness-shear mode and the mass loading onto the electrode surface was linear. He then derived the “Sauerbrey equation,” which had a significant influence on QCM. In the same year, QCM was firstly carried out on the mass sensor in the gas phase. In 1965, Mindlin and Lee made the thickness-shear and flexural vibrations of partially plated crystal plates [7]. And three years later, Bleustein et al [8] made the approximate solution under considering of the electrode mass.

In 1980s, the technique of QCM achieved a prominent advancement for which was improved to gauge in the liquid phase [9, 10]. For the recent decades, it had been extensively studied in promoting both of the energy trapping effect[11,12] and multi-channel quartz crystal microbalance [13]. The former one has great to do with the sensitivity of QCM and signal noise from environment when measuring. The latter one can determine several different analytes at the same time.

In 1995, Ishizaki et al [14, 15] tried diverse cutting and proved that the mesa design of QCM can harness the energy effectively to the electrode region and separate the thickness shear mode from the flexure mode. When Goka et al [16] investigated the energy trapping effect of bi-step mesa QCM in 2003, he concluded that the bi-step mesa design could reduce the impact by the boundary compared to the mesa design. In Lu et al’s [17, 18] discussion with finite elements analysis, 2005, they also found out the design would enhance the trapped energy when it was under the electrode region from 60% to 94%. In the same year, Shen et al [19] discussed the influence of the dual- electrodes design. They found the electrodes space caused the frequency drift, and it decreases the accuracy of measurement. And the mesa design has the same trend[20, 21]. In 2007, Pantalei et al [22] had built four-channel QCM and presented the outcomes by experiment.

The ultimate goal of this thesis is to enhance the energy trapping effect by designs of mesa and bi-step and obtain the additional benefits of biosensor miniaturization and accuracy promotion along with it.

Chapter 2 Theory

2.1 Introduction of Piezoelectric Materials

Literally, piezoelectric is expressed as "compress" and "electricity." When a material is compressed, some electric current will occur. Yet, on the other hand, if we apply voltage to a material, its shape will be deformed.

Piezoelectric materials can be categorized into 32 point groups and 7 crystal systems which include triclinic, monoclinic, orthorhombic, tetragonal, trigonal, hexagonal and cubic.

2.2 Introduction of Piezoelectric Effect

Piezoelectric effect discovered by Jacques Curie and Pierre Curie is the conversion between mechanical energy and electrical energy. When there is no force exerted to the piezoelectric structure, the geometric centers of both the positive charges and negative charges will be at the same point, or otherwise. Such phenomenon results in electric dipole and, further, the dipole moment. There are two types of piezoelectric effect: direct piezoelectric effect and inverse piezoelectric effect.

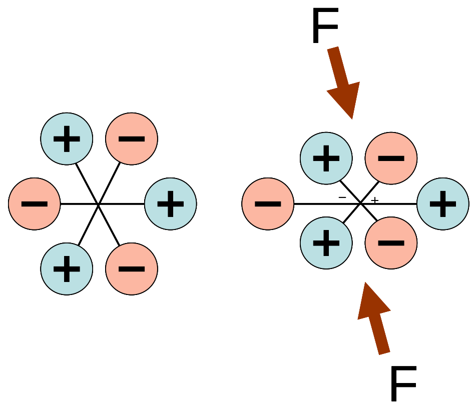

Fig 2. 1 Diagram of Crystal Structure Applying with External Force

2.2.1 Direct Piezoelectric Effect

With an external force, either compressed or extended, the piezoelectric material will lead to strain. In this case, the distance between diploes, or even polarization of the material, will be changed. Some of the surface bounded charges will then be released. The process is acknowledged as discharge. The transformation from mechanical energy to electrical energy is called the direct piezoelectric effect.

2.2.2 Inverse Piezoelectric Effect

In contrast to direct piezoelectric effect, when a material is applied to an electric field, piezoelectric material will be either compressed or extended alongside the direction over which the electric field is performed. When polarization of the material is in the same direction as the applied electric field, polarization gets stronger; dipole moment gets larger and the material is extended. When polarization of the material is in the opposite direction against the applied electric field, polarization gets weaker; dipole moment gets shorter and the material is compressed. The transformation from electrical energy to mechanical energy is called the inverse piezoelectric effect.

2.3 Introduction of Quartz

In the thesis, the α quartz of 32 point groups is what we adopted. The axis of α quartz is Z axis. The character of the quartz will alter based on different cutting directions. For now, the AT-cut quartz with the cutting angle of 35.15 degrees is chosen. See the graphics below.

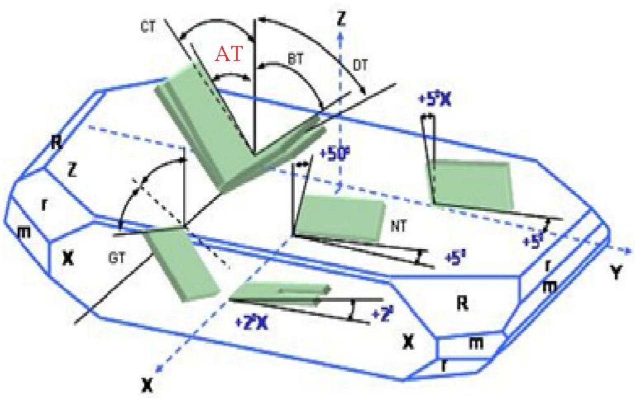

Fig 2. 2 Quartz Crystal with Different Cutting Angles

About AT-cut quartz, it has low variation induced by the temperature and can preserve steady resonance frequency at room temperature. This is why many electronic components operated at a high frequency would utilize AT-cut quartz as a vibrator.

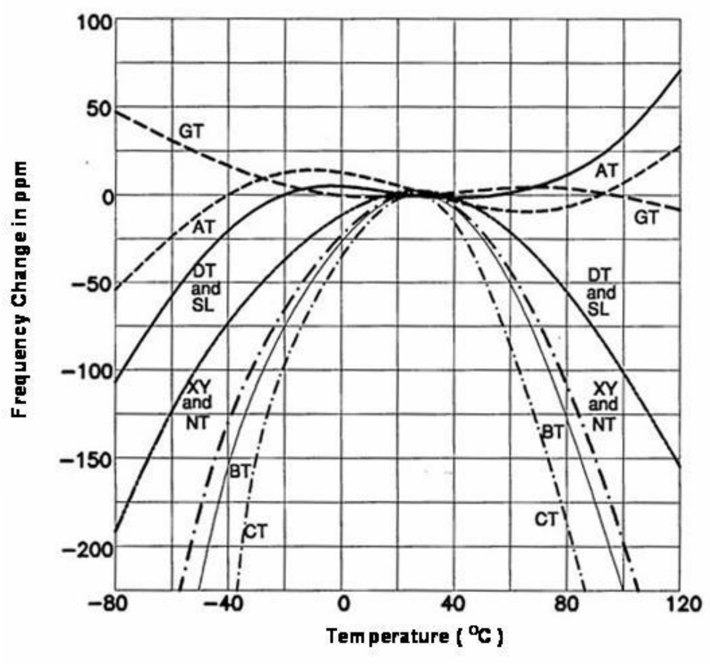

Fig 2. 3 Temperatures Influence of Quartz Crystal with Different Cutting Angles

2.4 QCM Working Principles

QCM (Quartz Crystal Microbalance) consists of a thin quartz crystal plate and two electrodes plated on its surface. With inverse piezoelectric effect, when positive electric field is inputted, the dipole will be attracted and that leads to the shear deformation. On the contrary, negative electric field will provoke the inverse direction shear deformation. If the same method is patterned after high frequency alternating current, the frequency of the thickness-shear mode will occur. Once the electric field frequency equals to the resonance frequency of the quartz, the quartz will reach the maximum vibration.

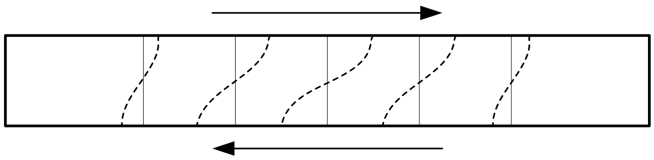

Fig 2. 4 Diagram of Thickness-shear Mode

With the mass loading onto the electrode surface increasing, the resonance frequency of the QCM thickness-shear mode will decrease relatively. From this phenomenon, we can calculate the mass on the electrode surface via the variation of the QCM resonance frequency. In general, the sensitivity of QCM can come to 1ng/Hz. In other words, 1 Hz variation of the resonance frequency attributes to 1 nano gram mass loading.

2.5 Frequency Drift Induced by Mass Loading

In 1959, Sauerbrey derived the equation about the relation of frequency shift and mass loading. If we consider a piezoelectric plate as demonstrated below,

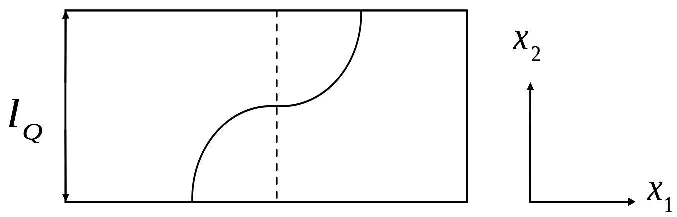

Fig 2. 5 Diagram of 2D QCM without Mass Loading

the condition of forming stationary wave will be

$$l_Q = n\left(\frac{\lambda_Q}{2}\right) \quad n=1,3,5,, \tag{2.5.1}$$

l_Q = thickness of quartz crystal

λ_Q = wave length

When n=1, the corresponding frequency is the fundamental one. An acoustic wave velocity is constant in the same medium as the following.

$$V_{tr} = \sqrt{\frac{\mu_Q}{\rho_Q}} \tag{2.5.2}$$

V_{tr} = wave velocity

μ_Q = shear module of quartz crystal

ρ_Q = density of quartz crystal

From $V_{tr} = f_Q \lambda_Q$ and $l_Q = \frac{\lambda_Q}{2}$, we can get the conclusion of

$$f_Q = \frac{V_{tr}}{2l_Q} \quad n=1 \tag{2.5.3}$$

Now, we assume the mass loading on the surface as the following.

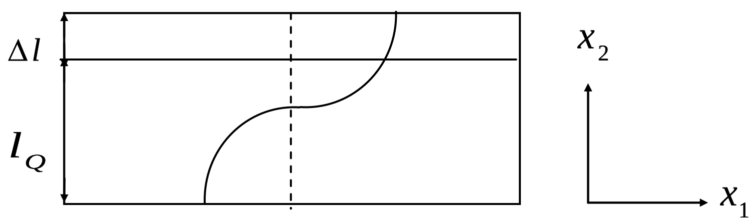

Fig 2. 6 Diagram of 2d QCM with Ideal Mass Loading

The condition of forming stationary wave becomes

$$\Delta l + l_Q = n\left(\frac{\lambda_Q}{2}\right) \quad \text{n=1,3,5,,} \tag{2.5.4}$$

According to equation (2.7.1) and (2.7.4), we can ascertain the fact that the length of stationary wave is getting longer. With the same medium, the wave velocity does not change.

$$V_{tr} = \frac{2\left(f_Q l_Q\right)}{n} = \frac{2\left(f_Q + \Delta f\right)\left(l_Q + \Delta l_Q\right)}{n} \tag{2.5.5}$$

When $\Delta f_Q \Delta l_Q \sim 0$, equation (2.7.5) becomes

$$\frac{\Delta f}{f_Q} = -\frac{\Delta l_Q}{l_Q} \tag{2.5.6}$$

In accordance with the assumption of Sauerbrey, the density of the mass loading is identical to quartz.

$$\frac{\Delta f}{f_0} = -\frac{\Delta l}{l_0} = -\frac{\dfrac{\Delta M}{A\rho_Q}}{\dfrac{V_{tr}}{2f_Q}} = -\frac{2f_Q}{A\rho_Q V_{tr}}\Delta M \quad \text{n=1} \tag{2.5.7}$$

A= area of electrode

ΔM = mass loading

From $V_{tr} = \sqrt{\dfrac{\mu_Q}{\rho_Q}}$, equation (2.7.7) becomes

$$\Delta f = -\frac{2f_Q^{\ 2}}{A\sqrt{\rho_Q \mu_Q}}\Delta M \quad \text{n=1} \tag{2.5.8}$$

There are some assumptions to work on.

1. The mass loading should adhere to quartz surface uniformly and tightly.

2. The mass loading has the same physical property with quartz.

With regard to the assumptions above and the property of quartz,

ρ_Q = quartz density =2.65g/cm^3

μ_Q = shear modules =2.95×10^{11} dyn/cm^2

we can calculate the frequency to get the mass loading by the equation below.

$$\Delta f = -2.3\times10^{-6} f_0^{\,2} \frac{\Delta M}{A} \tag{2.5.9}$$

2.6 Governing Equation

Concerning elastic materials, the equation of motion and the relation of displacement and strain can be expressed as follows.

$$\sigma_{ij,j} + f_i = \rho \ddot{u}_i \tag{2.6.1}$$

$$\gamma = \frac{1}{2}(u_{i,j} + u_{j,i}) \tag{2.6.2}$$

Where σ = stress tensor

u = displacement vector

γ = strain tensor

f = body force

In accordance with the assumption of quasi-static and the irrotational electric field, the Maxwell equation can be simplified as below.

$$D_{i,i}=0 \tag{2.6.3}$$

$$e_{ijk}E_{k,j} = 0 \tag{2.6.4}$$

$$E = -\phi_{,i} \tag{2.6.5}$$

Where D= electric displacement

E= electric field

ϕ = electric potential

Relating to the discussion of the constitutive law about piezoelectric materials in the concept of energy conservation, the piezoelectric materials' internal energy per volume unit can be expressed as

$$dU = dU_{elas} + dU_{elec} = \sigma_{ij}d\gamma_{ij} + E_i dD_i$$
$$\sigma_{ij} = \frac{\partial U}{\partial \gamma_{ij}}, E = \frac{\partial U}{\partial D_i} \tag{2.6.6}$$

U = total internal energy density

U_{elas} = strain energy density

U_{elec} = electric energy density

We introduce the Gibbs free energy function,

$$G = U - \sigma_{ij}\gamma_{ij} - E_i D_i \tag{2.6.7}$$

and combine equation (2.6.6) and (2.6.7).

$$\gamma_{ij} = -\frac{\partial G}{\partial \sigma_{ij}}, D_i = -\frac{\partial G}{\partial E_i} \tag{2.6.8}$$

We take Taylor expansion of γ_{ij} and D_i with respect to $\sigma_{ks} = \sigma_{ks}^0$ and

$E_k = E_k^0$.

$$\gamma_{ij} = \gamma_{ij}^0 + \frac{\partial \gamma_{ij}}{\partial \sigma_{ks}}(\sigma_{ks} - \sigma_{ks}^0) + \frac{\partial \gamma_{ij}}{\partial E_k}\left(E_k - E_k^0\right) + \cdots$$
$$D_i = D_i^0 + \frac{\partial D_i}{\partial \sigma_{jk}}\left(\sigma_{jk} - \sigma_{jk}^0\right) + \frac{\partial D_i}{\partial E_k}\left(E_k - E_k^0\right) + \cdots \tag{2.6.9}$$

Assume both of the initial stress and initial electric field equal to 0, it means $\sigma_{ks}^0 = 0, E_k^0 = 0$,

$$\gamma_{ij} = s_{ijks}^E \sigma_{ks} + \underline{d}_{ijk} E_k$$
$$D_i = d_{ijk}\sigma_{jk} + \varepsilon_{ik}^T E_k \tag{2.6.10}$$

and

$$s_{ilks}^E = \left.\frac{\partial \gamma_{ij}}{\partial \sigma_{ks}}\right|_E \quad \varepsilon_{\mathrm{ik}}^{\mathrm{T}} = \left.\frac{\partial D_i}{\partial E_k}\right|_\sigma \quad \underline{d}_{ijk} = \frac{\partial \gamma_{ij}}{\partial E_k} \quad d_{ijk} = \frac{\partial D_i}{\partial \sigma_{jk}} \tag{2.6.11}$$

s_{ilks}^E = the strain determined in constant electric field.

$\varepsilon_{\mathrm{ik}}^{\mathrm{T}}$ = the dielectric modules determined in constant stress

$\underline{d}_{ijk}$, d_{ijk} = Piezoelectric strain constants

The relation between $\underline{d}_{ijk}$ and d_{ijk} is shown below.

$$\underline{d}_{ijk} = \frac{\partial \gamma_{ij}}{\partial E_k} = -\frac{\partial^2 G}{\partial \sigma_{ij}\partial E_k} = -\frac{\partial^2 G}{\partial E_k \partial \sigma_{ij}} = \frac{\partial D_k}{\partial \sigma_{ij}} = d_{kij} \tag{2.6.12}$$

By equation (2.6.12), equation (2.6.10) turns to

$$\gamma_{ij} = s_{ijks}^E \sigma_{ks} + d_{kij} E_k$$
$$D_i = d_{ijk}\sigma_{jk} + \varepsilon_{ik}^T E_k \tag{2.6.13}$$

With Voigt's notation, we rewrite equation (2.6.13).

$$\begin{aligned} \gamma_p &= s^E_{pq}\sigma_q + d_{kp}E_k \\ D_i &= d_{iq}\sigma_q + \varepsilon^T_{ik}E_k \end{aligned} \qquad i, j, k = 1 \sim 3,\ p, q = 1 \sim 6 \tag{2.6.14}$$

If $p \le 3$, then $d_{kp} = d_{kij}$; if $p > 3$, then $d_{kp} = 2d_{kij}$.

Further, the expression of γ_p and D_i can be translated as σ_p and D_i

$$\begin{aligned} \sigma_p &= c^E_{pq}\gamma_q - e_{kp}E_k \\ D_i &= e_{iq}\gamma_q + \varepsilon^S_{ik}E_k \end{aligned} \tag{2.6.15}$$

c^E_{pq} = elastic modules in constant electric field

ε^s_{kp} = dielectric modules in constant strain

e_{kp} = piezoelectric modules

2.7 Fundamental Frequency of QCM

In 1968, Bleustein et al [8] derived approximation equation about the fundamental frequency of piezoelectric plate as follows. The directions of x_1 and x_3 are infinite, and the displacement is simply the function of x_2 as well as time. ρ and 2h represent the density and thickness of piezoelectric plate respectively while ρ_e and h_e stand for those of the electrodes. R is the ratio of electrode and piezoelectric plate ($R = \dfrac{\rho_e h_e}{\rho h}$).

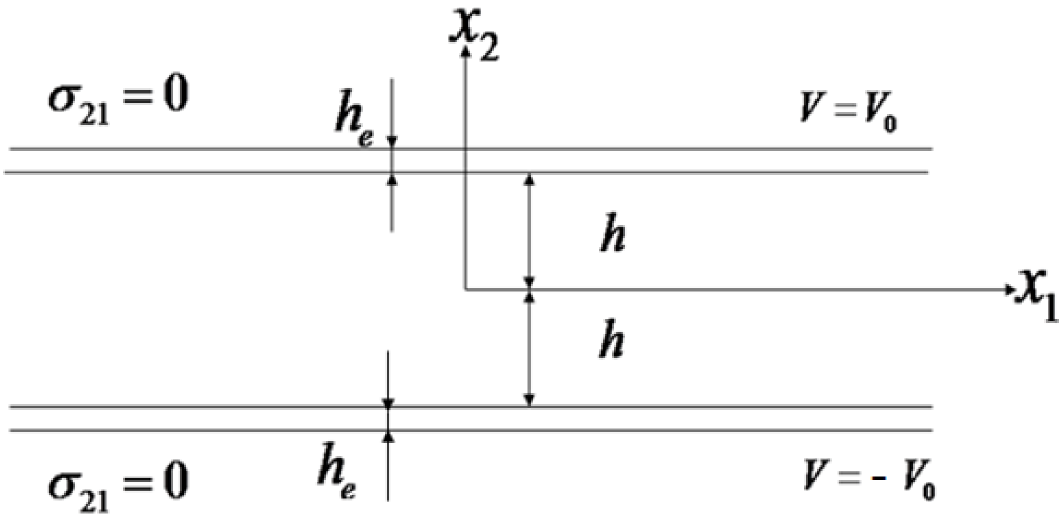

Fig 2. 7 2d QCM with Electrode Mass Model Diagram

From governing equation,

$$\begin{aligned}&\sigma_{21,2}=\rho\ddot{u}_1\\&D_{2,2}=0\end{aligned}\tag{2.7.1}$$

substitute equation (2.6.15), to equation (2.7.1),

$$\begin{aligned}&\sigma_{21,2}=c_{66}u_{1,22}+e_{26}V_{,22}=\rho\ddot{u}_1\\&D_{2,2}=e_{26}u_{1,22}-\varepsilon_{22}V_{,22}=0\end{aligned}\tag{2.7.2}$$

u_1 can be expressed as $u_1=u_1(x_2)e^{iwt}$. Equation (2.7.2) becomes

$$\begin{aligned}&\sigma_{21,2}=c_{66}u_{1,22}+e_{26}V_{,22}=-\rho w^2u_1\\&D_{2,2}=e_{26}u_{1,22}-\varepsilon_{22}V_{,22}=0\end{aligned}\tag{2.7.3}$$

From the second of equation (2.7.3),

$$V=\frac{e_{26}}{\varepsilon_{22}}u_1+a_1x_2+a_2\tag{2.7.4}$$

the boundary conditions are

$$\begin{aligned}c_{66}u_{1,2}+e_{26}V_{,2}\mp h_e\rho_e w^2u_1=0\quad&\text{at }\ x_2=\pm h\\V=\pm V_0\quad&\text{at }\ x_2=\pm h\end{aligned}\tag{2.7.5}$$

A solution satisfying the differential equation and the electric boundary conditions is worked out by

$$u_1 = A\sin\eta x_2 \tag{2.7.6}$$

Substituting the second of equation (2.7.5) and equation (2.7.6) into equation (2.7.4), it becomes

$$V = \frac{e_{26}}{\varepsilon_{22}} A(\sin\eta x_2 - \frac{x_2}{h}\sin\eta h) + \frac{V_0}{h} x_2 \tag{2.7.7}$$

where η must satisfy

$$\bar{C}_{66}\eta^2 = \rho\varpi^2 \tag{2.7.8}$$

$$\bar{C}_{66} = C_{66} + \frac{e_{26}^2}{\varepsilon_{22}} \tag{2.7.9}$$

The first of equation (2.7.5) becomes

$$A(\eta h\cos\eta h - k_{26}^2 \sin\eta h - R\eta^2 h^2 \sin\eta h) = \frac{e_{26}V_0}{\bar{C}_{66}} \tag{2.7.10}$$

Here, $k_{26}^2 = \dfrac{e_{26}^2}{\varepsilon_{22}\bar{C}_{66}}$.

The resonance occurs when the left term vanishes.

$$\tan\eta h = \frac{\eta h}{k_{26}^2 + R\eta^2 h^2} \tag{2.7.11}$$

And let $\eta h = \dfrac{\pi}{2} - \Delta$, Δ is a small quantity. Substitute it into equation (2.7.11).

$$\frac{\cos\Delta}{\sin\Delta} = \frac{\frac{\pi}{2} - \Delta}{k_{26}^2 + R(\frac{\pi}{4} - \pi\Delta + \Delta^2)} \tag{2.7.12}$$

Expand the trigonometric functions as power series in Δ and remember the rules of R<<1 and $k_{26}^2 << 1$ (for AT-cut quartz, $k_{26}^2 = 0.0078$).

$$\Delta^2 - \frac{\pi\Delta}{2} + k_{26}^2 + \frac{R\pi^2}{4} = 0 \tag{2.7.13}$$

The smallest root is

$$\Delta = \frac{2k_{26}^2}{\pi} + \frac{\pi R}{2} \tag{2.7.14}$$

So, we get the result that

$$\eta h = (\frac{\pi}{2})(1 - R - \frac{4k_{26}^2}{\pi^2}) \tag{2.7.15}$$

Substitute it to equation (2.7.8).

$$\varpi_0 = (\frac{\pi}{2h})(1 - R - \frac{4k_{26}^2}{\pi^2})(\frac{\bar{C}_{66}}{\rho})^{\frac{1}{2}} \tag{2.7.16}$$

Equation (2.7.16) is an approximate solution of 2D piezoelectric plate in consideration of the electrode mass loading. We will take this equation to test and verify our simulation result in chapter 3.

2.8 Energy Trapping Effect

Energy trapping effect is an important index of QCM measuring. Consider the dispersion curve of AT-cut thickness-shear wave and flexural wave shown below. $\bar{\Omega}$ is the dimensionless angle velocity and $\bar{\phi}$ is the dimensionless wave number; the curves without electric voltage are TS_1 and F_1, and those with electric voltage are TS_2 and F_2. The interception of $\bar{\Omega}$ -axis is called cut-off frequency.

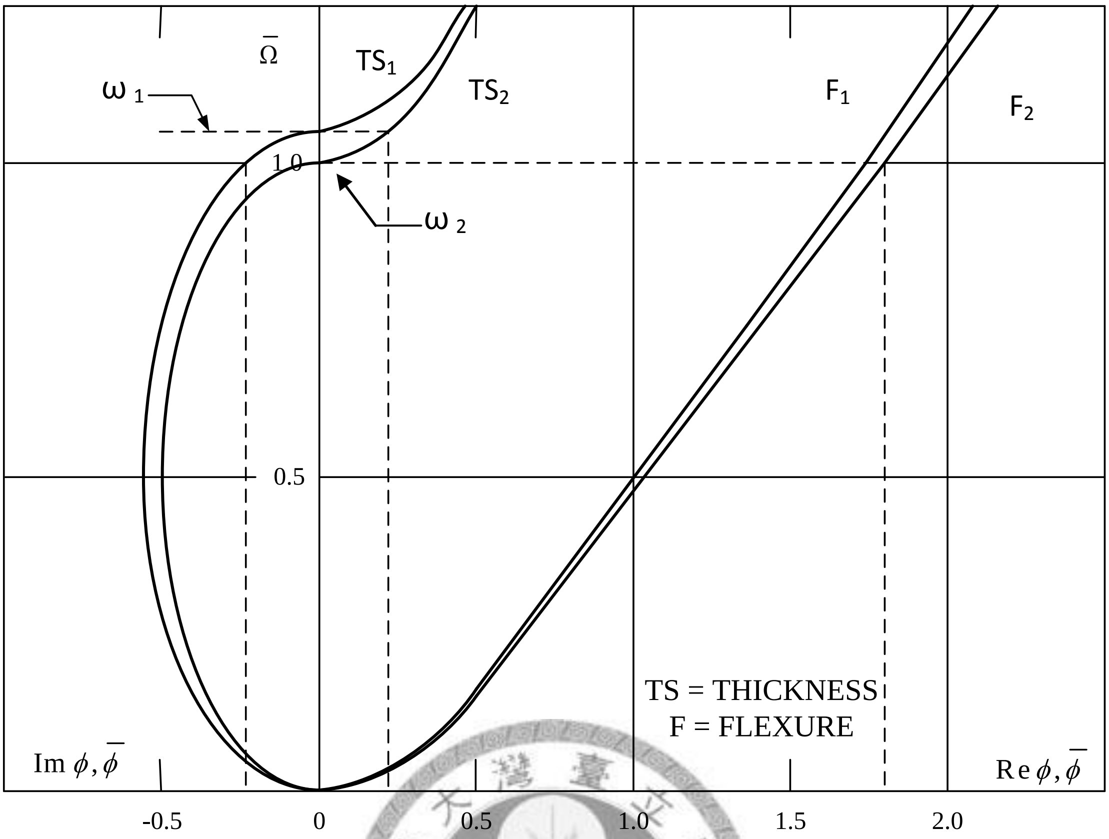

Fig 2. 8 Dispersion Curve of Basic QCM [5]

Generally, the resonance frequency of thickness-shear wave should locate between the region ω_1 and ω_2. When the AC frequency ω is between ω_1 (the region without electric voltage) and ω_2 (the region with electric voltage), the corresponding wave number for TS_1 is in the imaginary part, and that for TS_2 is in the real part. As for the vibration of thickness-shear mode, it is making simple steady motion in x1 direction. We express it by

$$u_x = A_m e^{i(wt + kx_1)} \tag{2.8.1}$$

Where u_x = displacement in x_1 direction

A_m= amplitude

w = vibration frequency

t= time

k= wave number

x= position of x_1 direction

With reference to equation (2.8.1), the region with electric voltage keeps on vibrating. However, the region without electric voltage presents the exponential decay with the position of x direction. These represent that the vibration occurs only in the region with electric voltage. That is to say, the energy will be trapped around electrode. This phenomenon is called energy trapping effect.

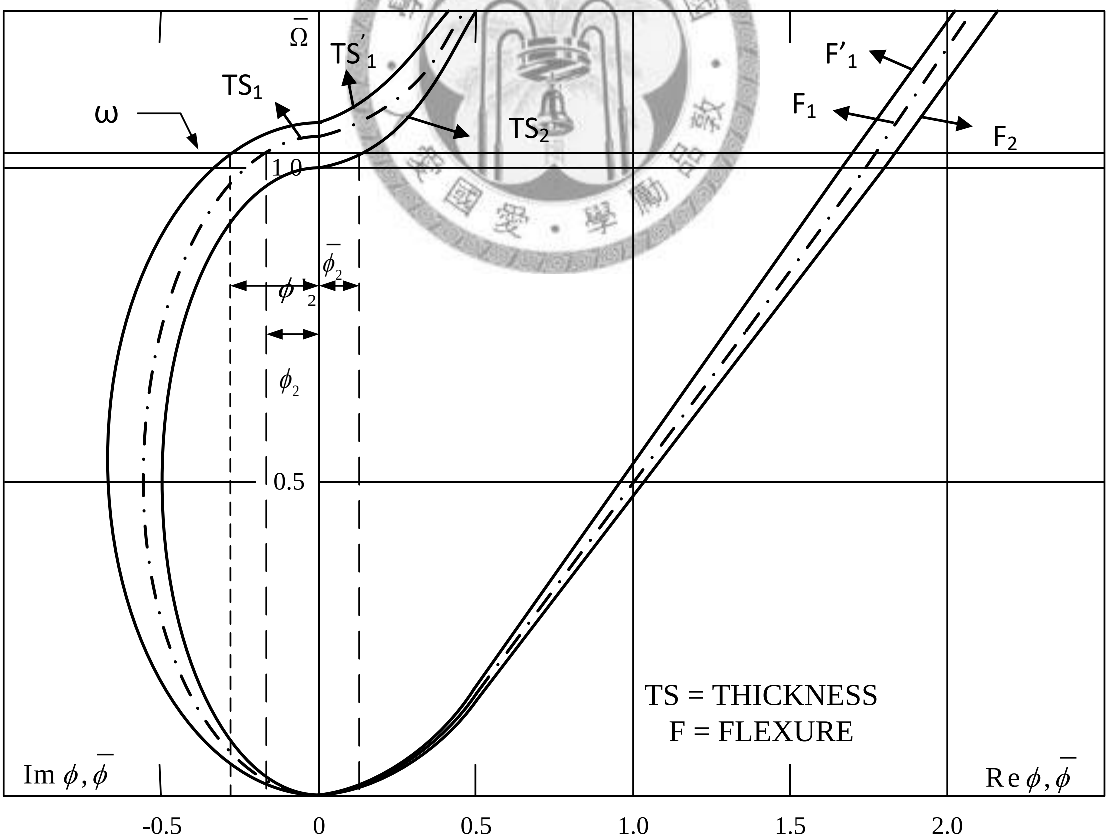

Fig 2. 9 Dispersion Curve of Mesa Design QCM

Fig2.9 gives the dispersion curve of mesa design. In the diagram, the curve of the region without electric voltage moves up to TS'_1 and F'_1 from TS_1 and F_1, in the same meaning, it moves to a continuous line from a dotted line. Without the mesa design, when the resonance frequency takes place, the distance of the cross point which is of the region without electric voltage in the dispersion curve is $\bar{\phi}_2$, of the region with voltage is ϕ_2. After the mesa design, the distance of the region with voltage increases to ϕ'_2, the region without voltage is still $\bar{\phi}_2$. It means that the region with voltage still keeps making harmonic vibration, and the region without voltage decays with the position of x direction more faster. Meanwhile, the energy trapping effect is more obviously.

The advantages of enhancing the energy trapping effect of QCM are:

1. Increase of sensitivity: To observe frequency variation will become much easier.
2. Increase of stability: It will amplify the amplitude of thickness-shear wave and diminish that of other types. Hence, the impact on measuring precision of thickness-shear wave will be more obvious than that of other types.

Accordingly, the stronger energy trapping effect is, the more excellent the performance of QCM can achieve. Efforts to upgrade energy trapping effect are our main target to improve QCM performance.

In our studies, it is the following index that we introduce to quantify the sensitivity of QCM.

$$\text{energy trapping factor} = \frac{\int E_{electrode}\,dv}{\int E_{all}\,dv} = \frac{\overline{K} + \overline{U}}{\overline{K} + \overline{U} + K + U} \tag{2.8.2}$$

For the purpose of comparison, we take the potential energy below into account.

$$\text{energy trapping factor} = \frac{\int E_{electrode}\,dv}{\int E_{all}\,dv} = \frac{\overline{U}}{\overline{U} + U} \tag{2.8.3}$$

Generally speaking, the entire vibration energy comprises the kinetic energy and the potential energy. In the study, thickness-shear wave causes time-harmonic deformation of a crystal. With the utmost deformation, the potential energy will reach to maximum but the kinetic energy will be zero. For this reason, we can neglect the influence of kinetic energy. [18]

Chapter 3 Two-dimensional Finite Element Analysis

3.1 Preface and Convergence Test

This research is conducted with the finite element analysis software, ABAQUS. Two-dimensional Models are plane stress problems. The element type for piezoelectric problem chosen here is CPE8RE (An 8-node plane strain piezoelectric quadrilateral, reduced integration). Models are subject to frequency analysis based on boundary condition of electric potential applied to the left electrode. Fig 3.1 shows when the mesh size is reduced, the corresponding variation of the resonance frequency of theoretical model (fig 2.7) becomes less. To keep a balance between accuracy and time-saving issue during simulation, mesh size of 0.012 was chosen.

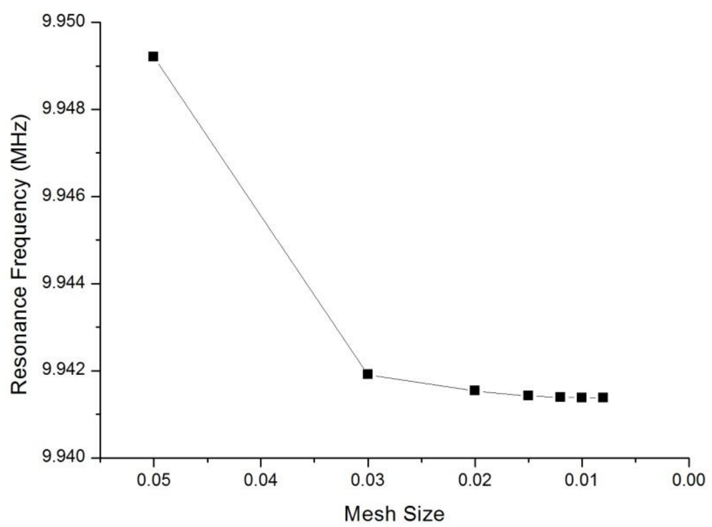

Fig 3. 1 Convergence Test for two-dimensional Simulation

3.2 Verification of Two-dimensional Theoretical Model

Tracing back the previous studies wrote by Bleustein et al [8], two-dimensional model frequency can be estimated through equation (2.7.16). The theoretical model is utilized to simulate by setting the x-direction boundary. And we found the error between the simulation and theory is 0.32% when the ratio of length and thickness is 400 times. Then we took advantage of the equation to compute the dual-channel QCM frequency by setting different electrode thickness in the thesis.

3.2.1 Verification of Two-dimensional Basic Dual-channel Model

Fig 3.2 is the simulation model we adopted. "L" is the length of the quartz crystal and "a" is the width of electrode; "b" is the distance from the quartz center to the electrode while "c" is from the quartz boundary to the electrode; "h" stands for the height of the quartz; "h_{e1}" and "h_{e2}" mean the height of left and right electrode respectively. With consideration of the settings of dimension, L = 8mm, a = 1mm, b = 0.5mm, c = 1.5mm, h = 0.0852mm, h_{e1}=0.1μm, we take h_{e2} as a variable to make a group of data with five parameters. In accordance with table 3.2, the error is nearly 0.7% for the left, and 1% for the right. Our simulation result is believable on account of the close outcome with the theory.

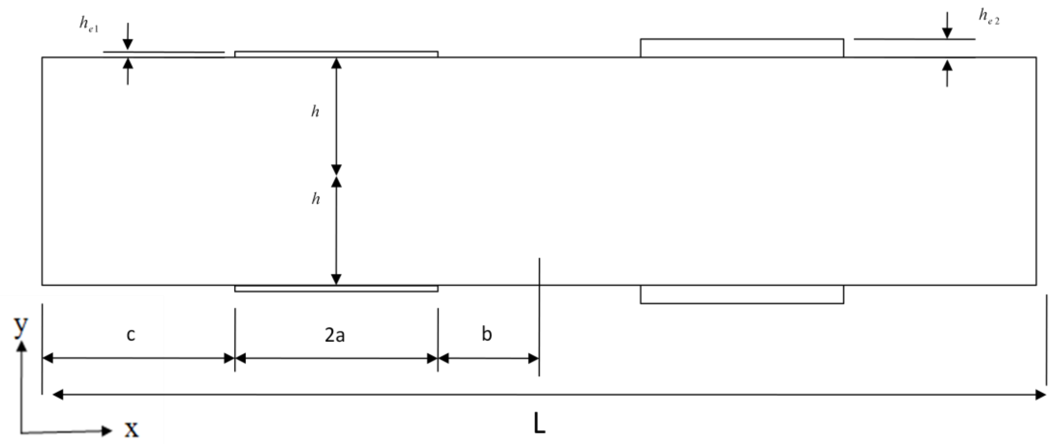

Fig 3. 2 Two-dimensional Basic Dual-channel Model

	h_{e1}	h_{e2}
data 1	0.1μm	0.2μm
data 2	0.1μm	0.25μm
data 3	0.1μm	0.3μm
data 4	0.1μm	0.35μm
data 5	0.1μm	0.4μm

Table 3. 1 Data with Five Parameters which Takes h_{e2} as a Variable

	Simulation frequency (MHz)		Theory frequency (MHz)		Error	
	left electrode	right electrode	left electrode	right electrode	left electrode	right electrode
data 1	9.973	9.903	9.903	9.819	0.7%	0.9%
data 2	9.971	9.866	9.903	9.777	0.7%	0.9%
data 3	9.965	9.83	9.903	9.735	0.6%	1.0%
data 4	9.977	9.793	9.903	9.693	0.7%	1.0%
data 5	9.975	9.756	9.903	9.651	0.7%	1.1%

Table 3. 2 Comparison of 2D Basic Dual-channel QCM between Simulation and Theory

3.2.1 Energy Trapping Effect of Two-dimensional Basic Model

The value of energy trapping factor represents the amount of the energy concentrating under the electrode region when QCM oscillates. The greater the value is, the more the energy centralizes. When the value comes to 1, the measurement is most accurate, because all energy is focused on the electrode region. In order to realize the influence on the vibration coupling effect from different distances between the electrodes, we suppose b as a variable and observe the variation of energy trapping factor. According to fig 3.7, where longitudinal axle is energy trapping factor and transverse axle is the distance between electrodes (i.e. “b”), energy trapping factor will increase with the expansion of distance between electrodes and reach to maximum till b=1.4mm. Afterward, it will start to diminish. In general, maximum should occur at the center of the quartz crystal (b=1mm) when there is no interference between electrodes. However, from the result of simulation, the coupling effect between electrodes is more powerful than boundary effect. We can then conclude that the distance between electrodes has a great effect on energy trapping factor and b is suggested staying at 1.4mm. Nevertheless, the theme of this research is to improve the efficacy of QCM under the assumption of small interval. Thus, b=0.5mm is the size for this thesis.

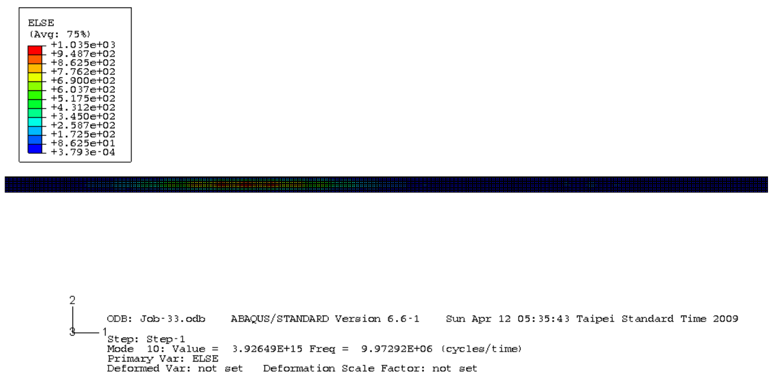

Fig 3. 3 Simulation Result for Left Electrode of 2D Basic Model

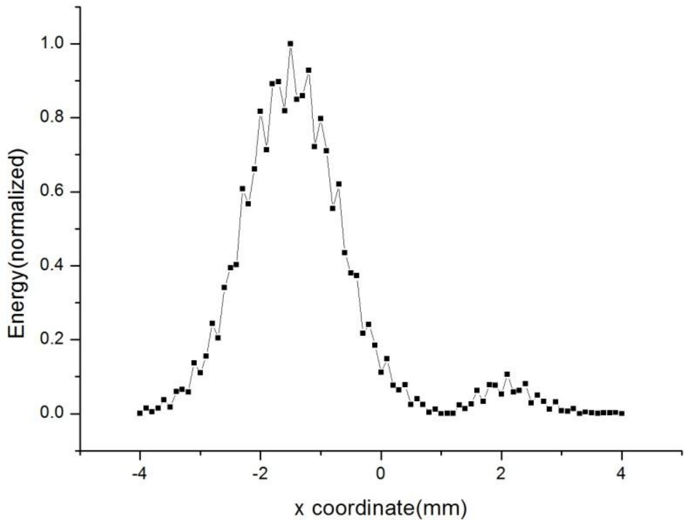

Fig 3. 4 Energy Diagram for Left Electrode of 2D Basic Model

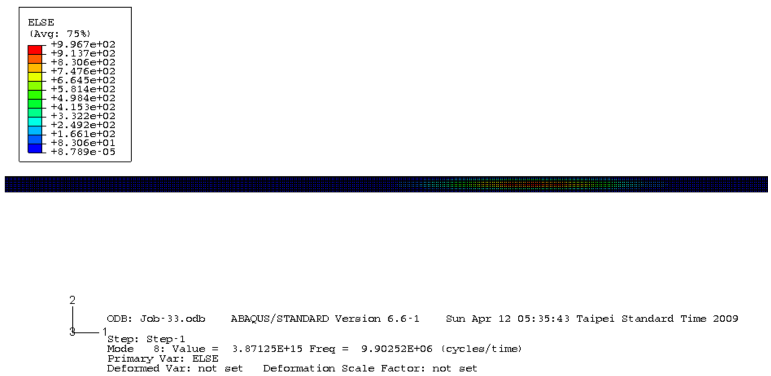

Fig 3. 5 Simulation Result for Right Electrode of 2D Basic Model

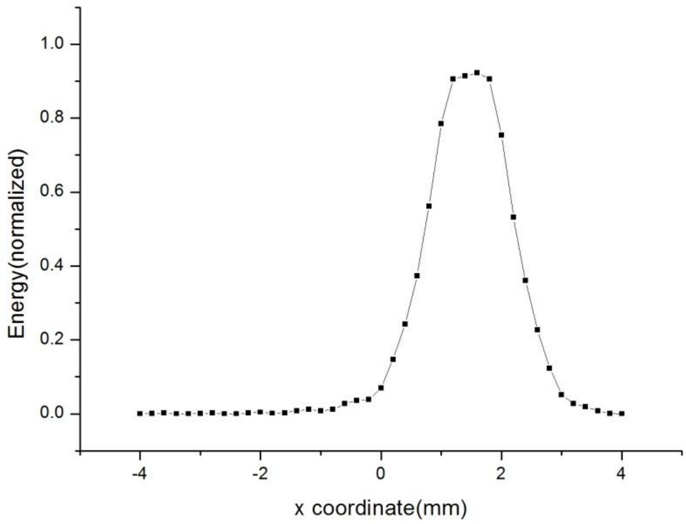

Fig 3. 6 Energy Diagram for Right Electrode of 2D Basic Model

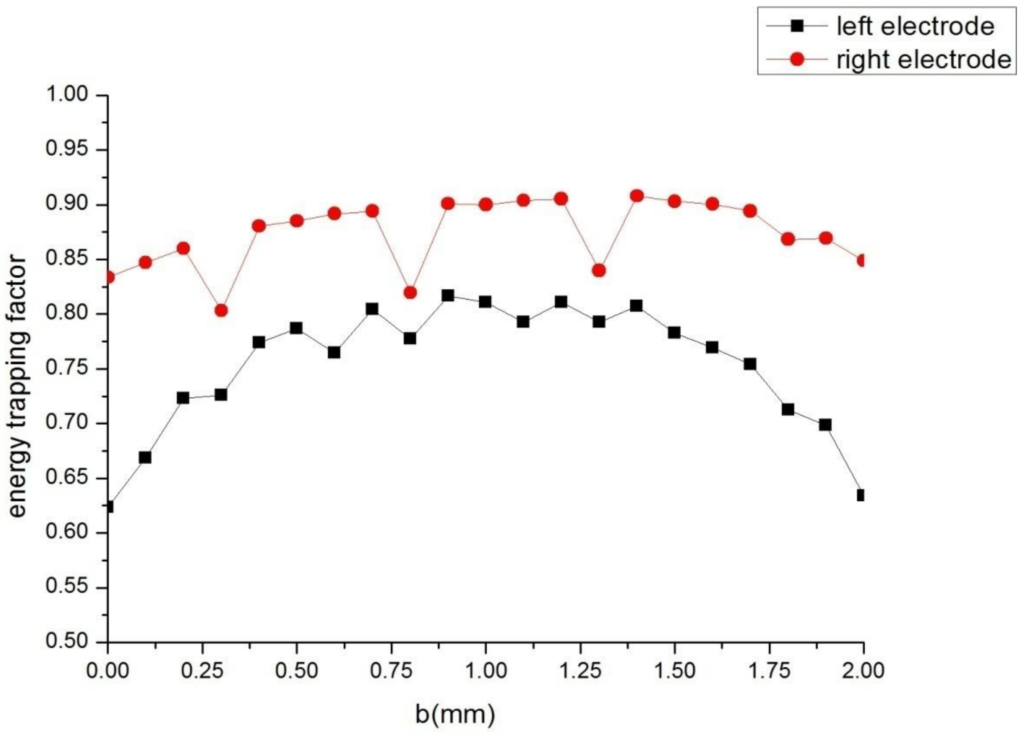

Fig 3. 7 Energy Trapping Curve with the Variable b

3.3 Two-dimensional Mesa Design

From the literature, the mesa design is introduced to harness the energy to the electrode region and separate the thickness shear mode from the flexure mode. This design is proved that it has superior efficiency to the basic. The simulation of mesa design is enforced to reappear its merit.

3.3.1 Two-dimensional Mesa Design Model

We compare the mesa design model, which is coductive to energy trapping effect, with the basic model. Fig 3.8 is the model for simulating, where “L” is the length of the quartz crystal and “a” is the width of electrode; “b” is the distance from the quartz center to the electrode while “c” is from the quartz boundary to the electrode; “h_1” and ”h_2” correspond to the height of the un-plated region and the electrode region each while “h_{e1}” and “h_{e2}” equal to the left and the right electrode respectively. Taking the settings of dimension into account, L = 8mm, a = 1mm, b = 0.5mm, c = 1.5mm, h_1 = 0.0852mm, h_{e1}=0.1μm, h_{e2}=0.2μm, we then introduce a variable “δh”, which means the mesa height, $\delta h=h_1-h_2$

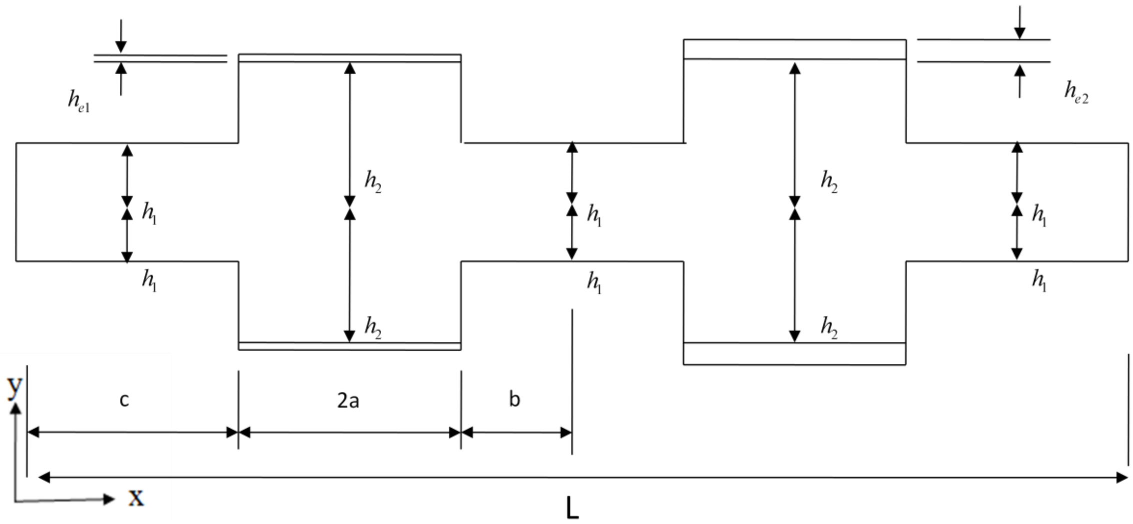

Fig 3. 8 Two-dimensional Mesa Design Model

3.3.2 Energy Trapping Effect of Two-dimensional Mesa Design Model

In fig 3.9 and 3.10, the transverse axle is the height of the mesa and the longitudinal axle is energy trapping factor. Ignoring the non-continuous point dropping abruptly, we detect a positive trend of the value of energy trapping factor as the increase of the mesa height (δ h) and most mesa designs are shown superior to basic model. All mentioned above verify the assumption that the performance of vibration concentration can be promoted effectively due to mesa design. However, the height should be limited to δh> 25μm rather than elevate infinitely.

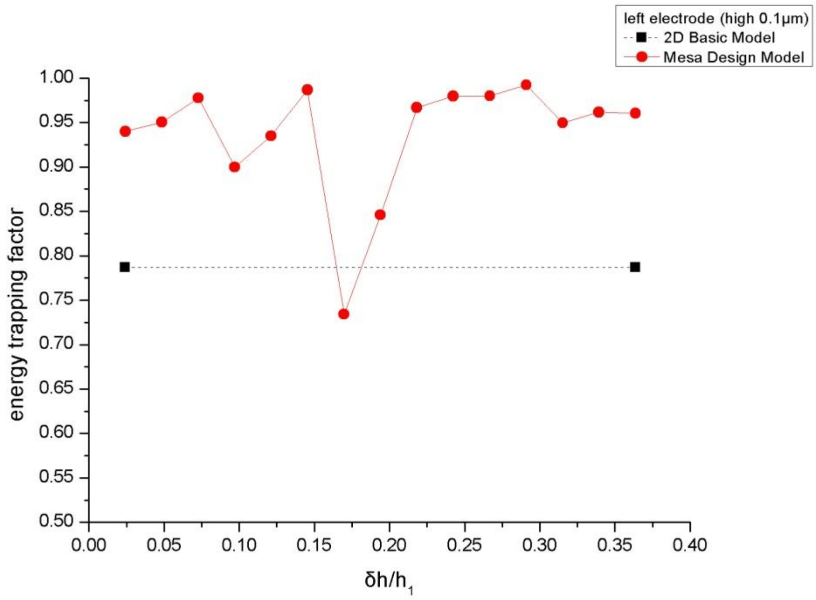

Fig 3. 9 Energy Trapping Curve with Variable δh for Left Electrode of 2D Basic Model and Mesa Design Model

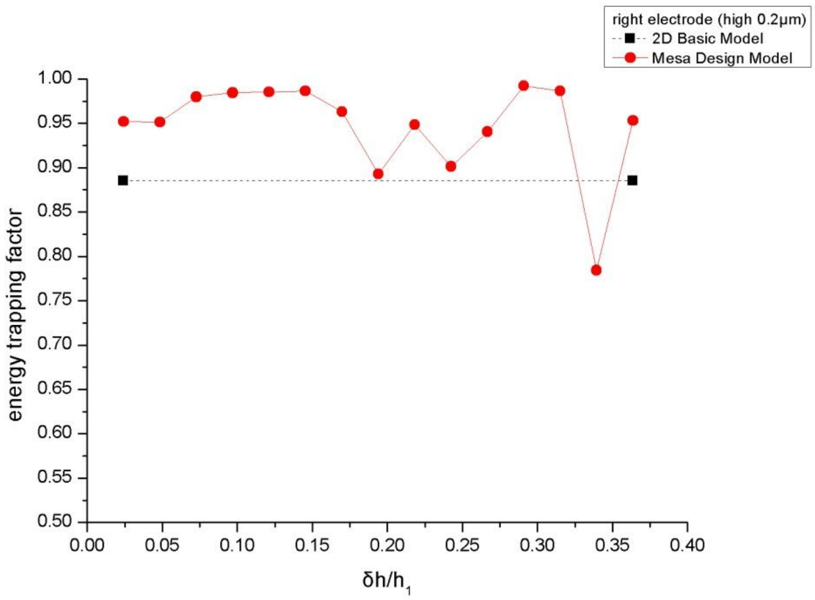

Fig 3. 10 Energy Trapping Curve with Variable δh for Right Electrode of 2D Basic Model and Mesa Design Model

3.3.3 Interval Frequency of Two-dimensional Mesa Design Model

So as to distinguish the the mass loading between left and right electrode clearly, there ought to maintain a certain fequency interval. Therefore, it is also a vital topic to discuss about the drift of frequency with regard to various designs in addtion to the presentation of energy trapping factor.

In fig 3.11, the transverse axle is the height of the mesa and the longitudinal axle is the resonance frequency. Red and black curve are right and left electrode each. Whenever we raise the height of mesa, the responding resonance frequency will get negtive reaction linearly. We can discover the same in the fig 3.12 where the frequency difference between right and electrodes is δf namely $\delta f = f_{left} - f_{right}$.

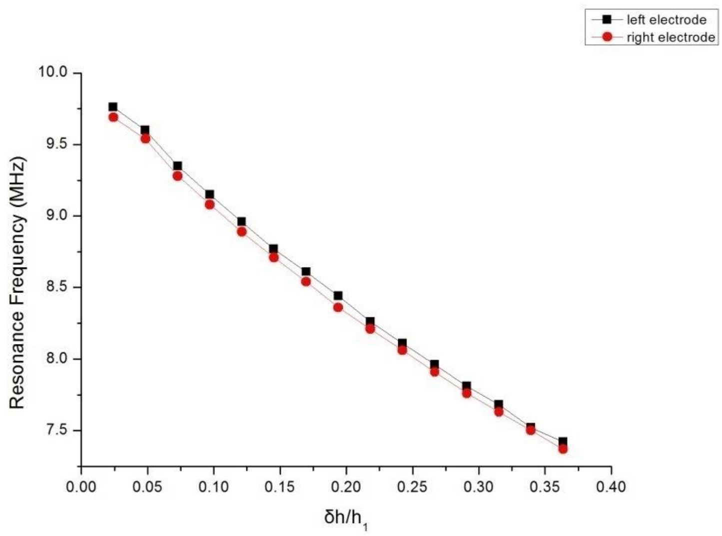

Fig 3. 11 Resonance Frequency with Variable δh

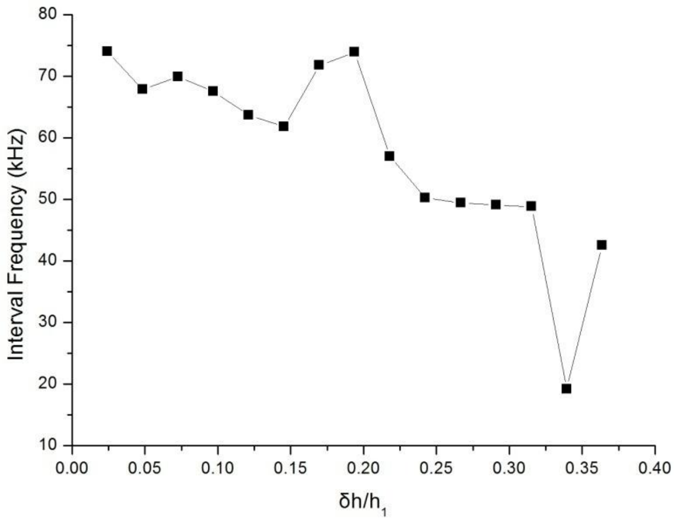

Fig 3. 12 Interval Frequency with Variableδh between Two Electrodes

3.3.4 Investigation of Dropping Effect

From the simulation results in the previous chapters, we notice that the occurrence of dropping effect has an extremely impact for the optimization in design, for it is not only unpredictable but also will decrease the energy trapping factor. Therefore, once the reason of such phenomenon can be identified, it will be greatly beneficial on our design.

According to the literature [23], Shockley et.al conjectured that the coupling between thickness shear wave and flexure wave due to the finite boundary of the crystal results in the dropping effect. Since the vibration of flexure wave is in the y-direction, we restrict the displacement in such direction. Namely, we eliminate the incident of flexure wave to calculate the corresponding energy trapping factor

As shown in Fig 3.13, we constrain the y-displacement on the lower and upper sides of boundaries in un-electrode regions of 2D mesa model (Red parts in the model) and then test once more.

From the Fig3.14 and Fig3.15, the occurrence of dropping points disappears thoroughly after the limitation on the y-displacement. Hence, the fact is certified that the appearance of dropping points can be avoided by suppressing the flexural wave effectively.

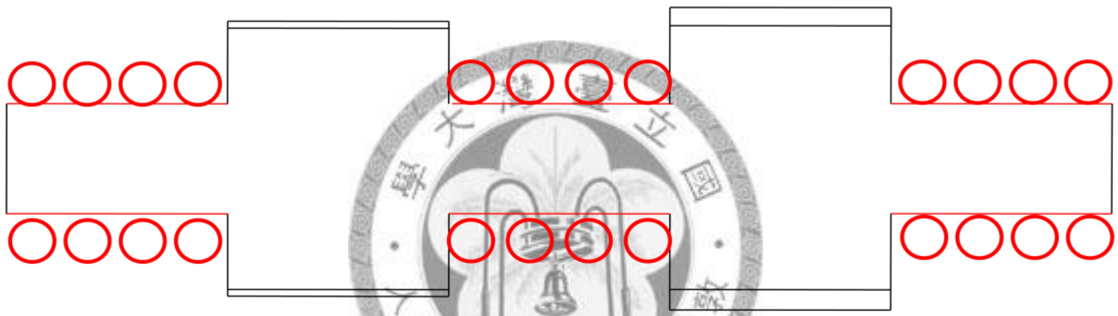

Fig 3. 13 2D Mesa Model with Y-displacement Constrain

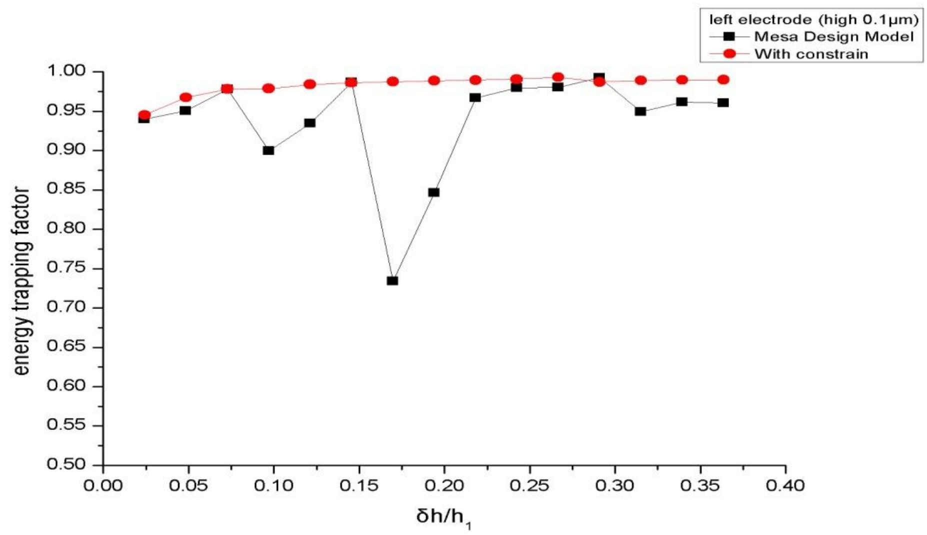

Fig 3. 14 Energy Trapping Curve for Left Electrode with Y-displacement Constrain

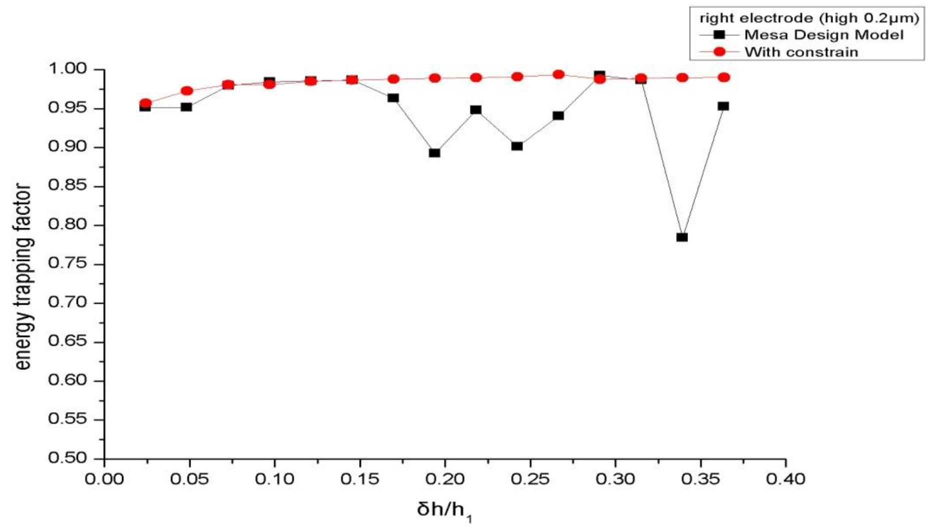

Fig 3. 15 Energy Trapping Curve for Right Electrode with Y-displacement Constrain

國立臺灣大學 · 敬業樂群 · 愛國愛人

Chapter 4 Three-dimensional Finite Element Analysis

4.1 Preface and Convergence Test

The setting boundary of the three-dimensional analysis is the same as the two-dimensional one and the difference comes to the consideration of the dimension in z-direction and the chosen element type. The chosen element type for three-dimensional simulation is C3D20RE, which is a 20-node piezoelectric quadrilateral, reduced integration element. Based on the two-dimensional model, we move on to our topic about the three-dimensional assumption and figure out how the responding energy trapping effect as well as the interval frequency work when the three distinct models are extended from two-dimensional models. Fig 4.1 shows the convergence test of three-dimensional simulation. The mesh size of 0.14 is chosen.

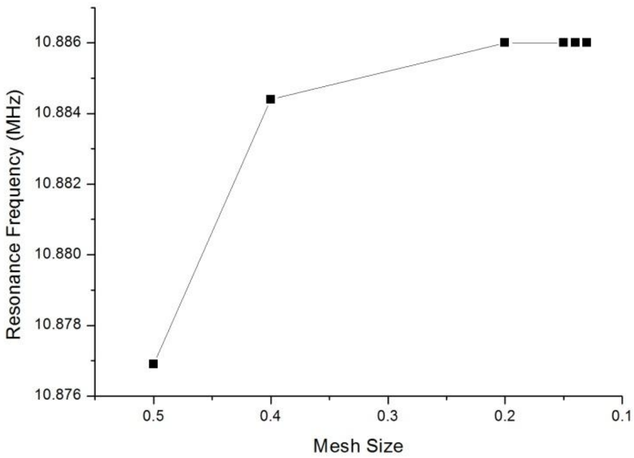

Fig 4. 1 Convergence Test for three-dimensional Simulation

4.2 Three-dimensional Basic Dual-channel Design

In accordance with the two-dimensional plane strain problem, the original three-dimensional diagram should be in the form of beam when it is developed. Furthermore, QCM is ordinarily made into a circular-shaped plate. Hence, after taking the factors into consideration and to avoid unnecessary complications in the analysis, the three-dimensional diagram is set to a rectangle-shaped plate. Fig 4.2 demonstrates how a 2d diagram is developed into a 3d one. The section of XY-plane skecth is equavenlent to Fig 3.1 when the dimension of z-coordinate equals 0. The shape of the XZ-plane is square, which means the length of z-direction is equal to the length of x-direction. The corrsepoding dimension we use here is h_{e1}=0.1μm, h_{e2}=0.2μm, 8mm for the length on z-direction and the other settings are equivalent to the two-dimensional basic model.

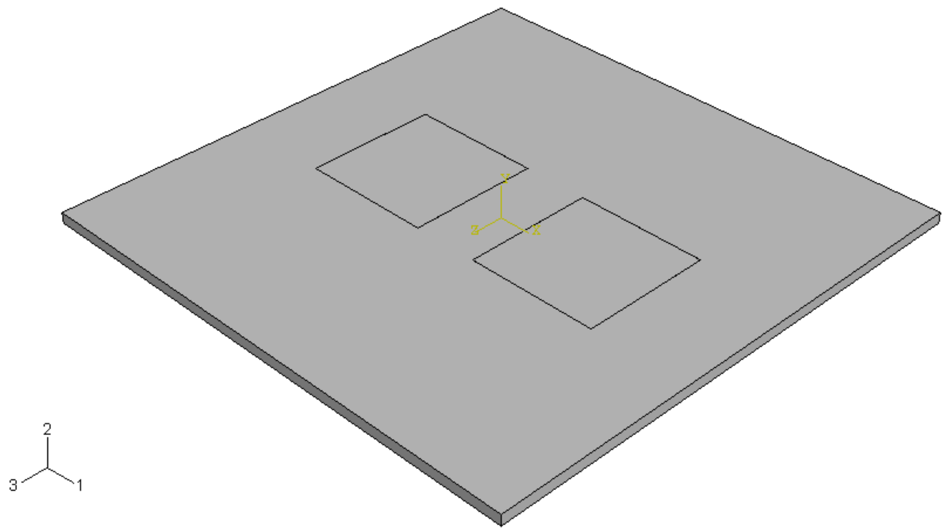

Fig 4. 2 Sketch of Three-dimensional Basic Dual-channel Model

4.2.1 Result of Three-dimensional Basic Dual -channel Model

From Fig 4.2 and 4.3, the energy diagrams of the three-dimensional basic model, we notice that the distribution of energy trapping is identical to the two-dimensional model which is the closer it gets to the electrode core, the higher the energy density is. Its corresponding energy trapping effect is 0.836 for the left electrode and 0.944 for the right. The resonance frequency is 10.987MHz for the left and 10.885MHz for the right, and the interval frequencyδ f is 10200Hz.

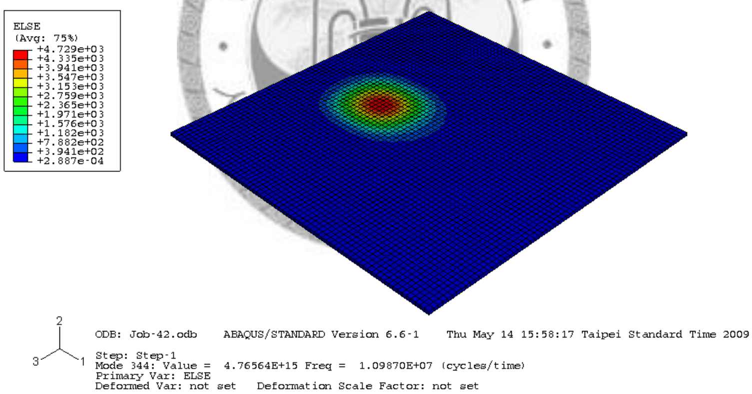

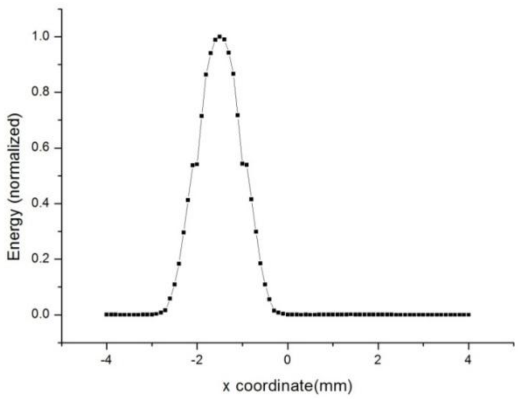

Fig 4. 3 The Energy Diagram for the Left Electrode of 3d Basic Model

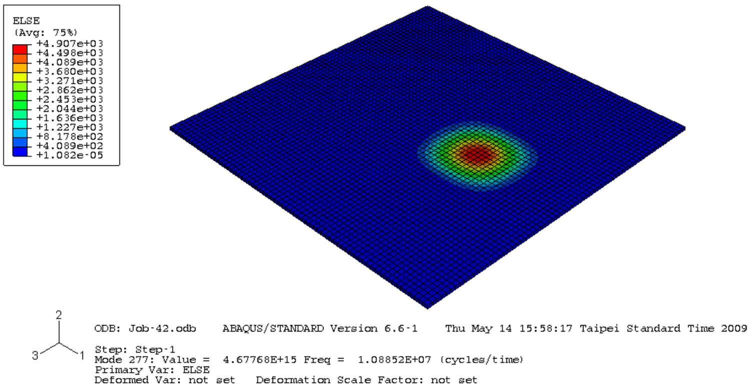

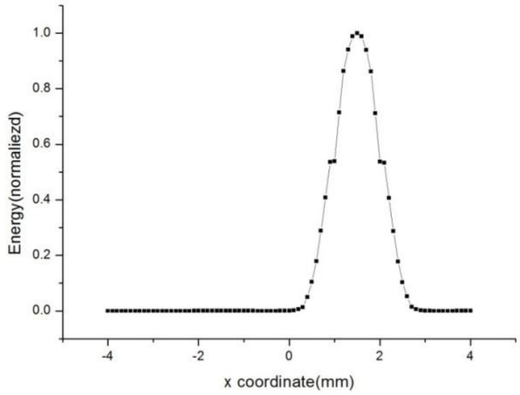

Fig 4. 4 The Energy Diagram for the Right Electrode of 3d Basic Model

4.3 Three-dimensional Mesa Design

In the previous chapters, the effect of mesa design is proven by the two-dimensional simulation; meanwhile, the occurrence of drop point, which is unpredictable, is noted. In this chapter, the three-dimensional model is employed to resemble the reality. The XY-plane sketch of the three-dimensional model we use here is as what Fig 3.6 demonstrates. Within the premise of the same XY-plane and the consideration of the plane strain problems, the following three 3D models are developed.

4.3.1 Three-dimensional Mesa Design –Model 1

As shown in Fig 4.5 and 4.6, model 1, the common sketch for three-dimensional mesa design, is composed of a quartz plate and a quartz mesa, which has the same size with the electrode. Both the thickness of electrodes as well as the dimension of the quartz plate chosen here correspond to that of the three-dimensional basic model except the height of mesa. And the simulation results are shown below.

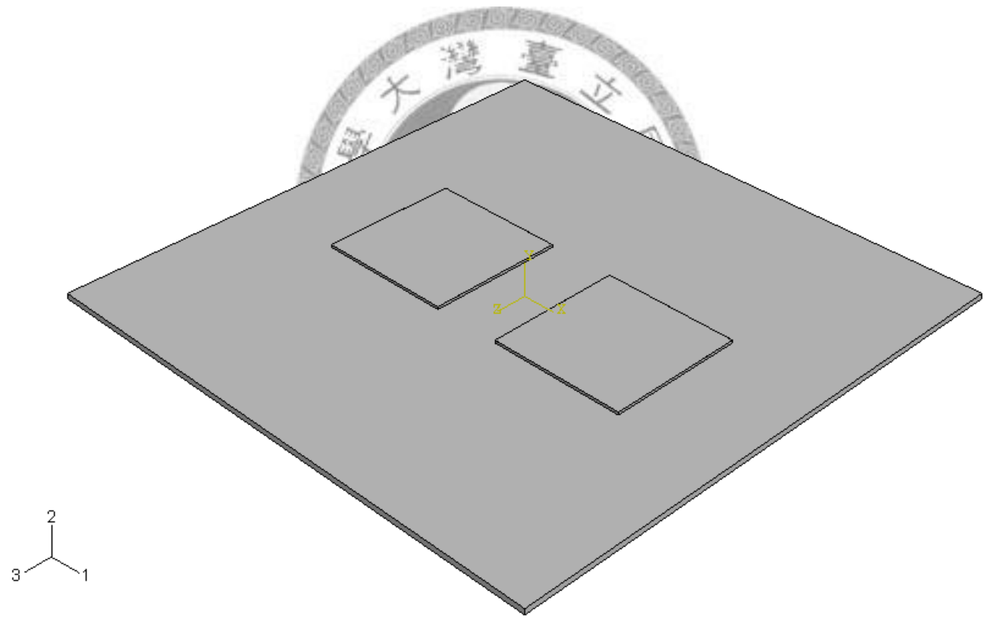

Fig 4. 5 Sketch of Model 1

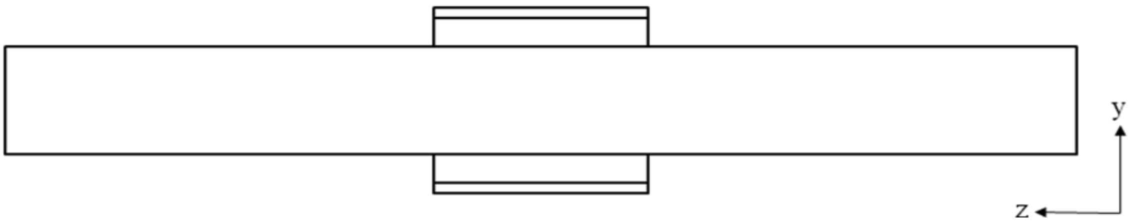

Fig 4. 6 YZ-plane Sketch of Model 1

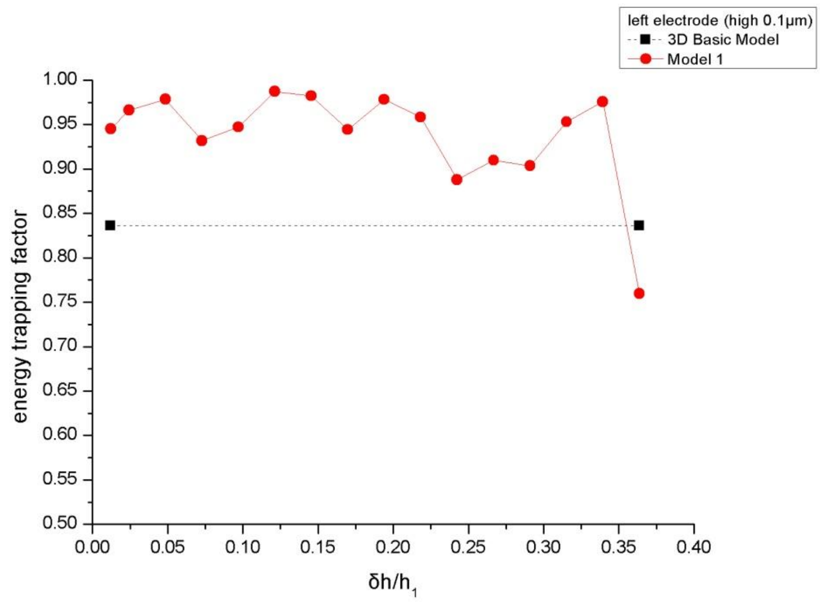

Fig 4. 7 Energy Trapping Curve of Model 1 Left Electrode

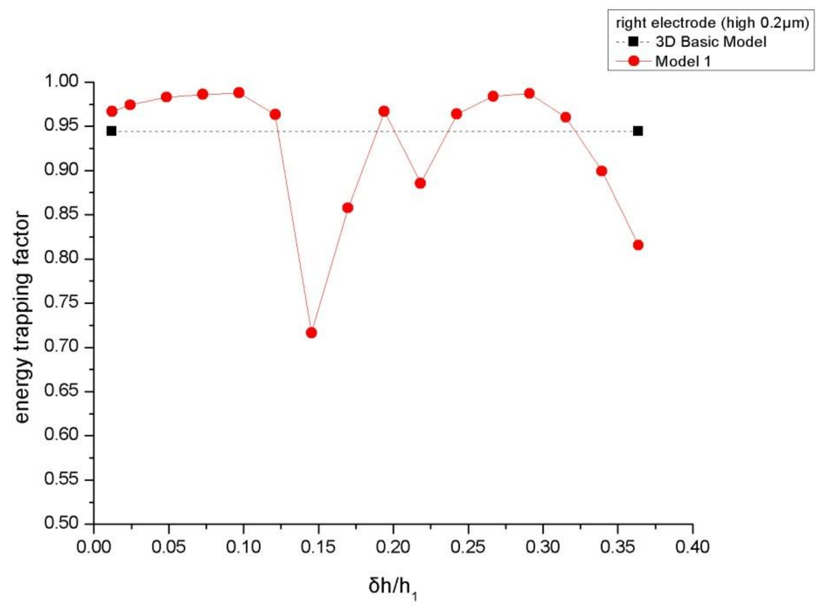

Fig 4. 8 Energy Trapping Curve of Model 1 Right Electrode

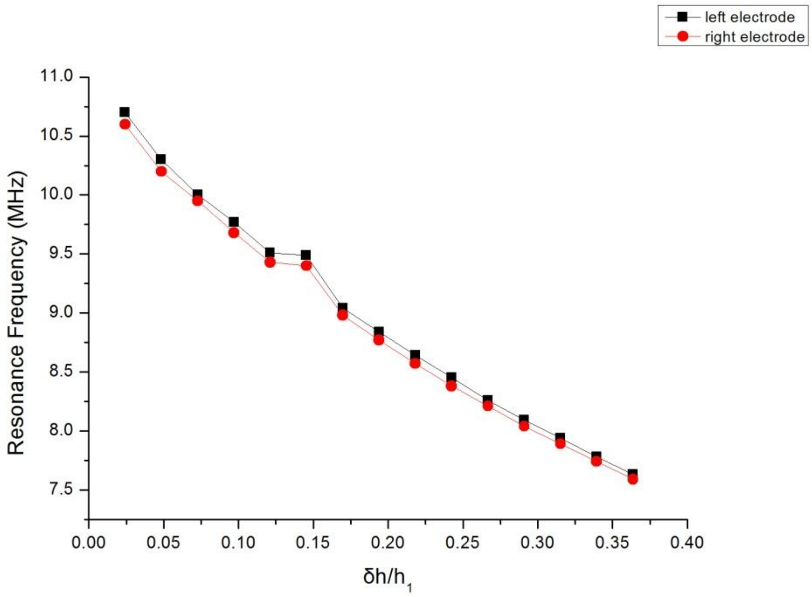

Fig 4. 9 Resonance Frequency of Model 1

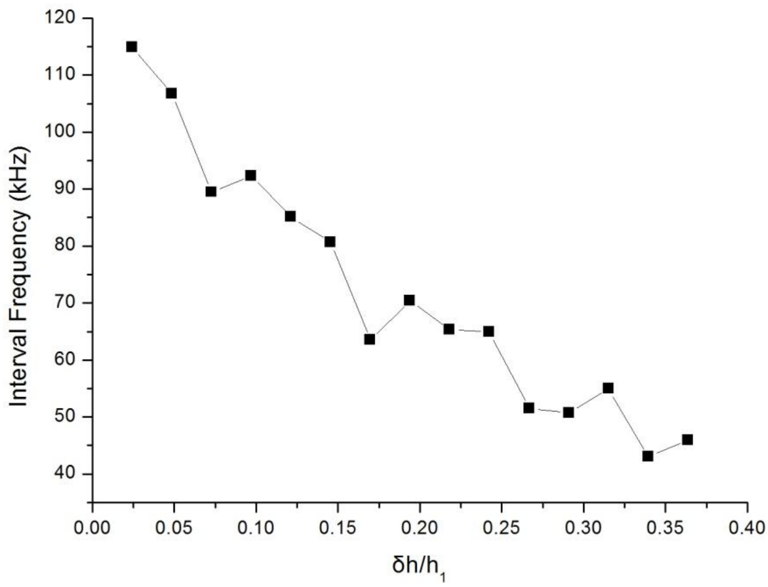

Fig 4. 10 Interval Frequency of Model 1

4.3.2 Three-dimensional Mesa Design –Model 2

As shown in Fig 4.11 and 4.12, model 2 is the sketch extending the original quartz along the z-direction and turning the electrode to be square. But the dimension of electrode excluding the height of mesa remains constant with the three-dimensional basic model. And the simulation results are shown below.

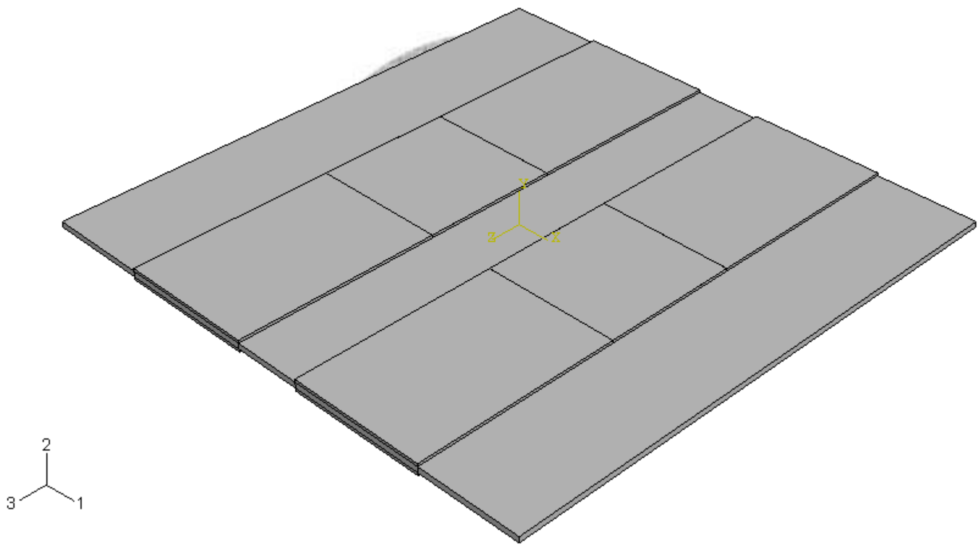

Fig 4. 11 Sketch of Model 2

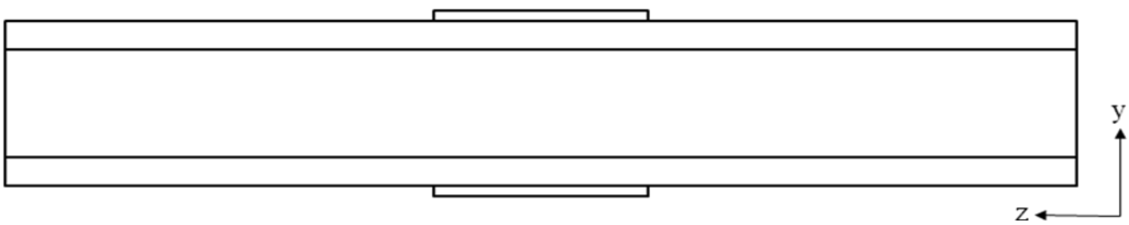

Fig 4. 12 YZ-plane Sketch of Model 2

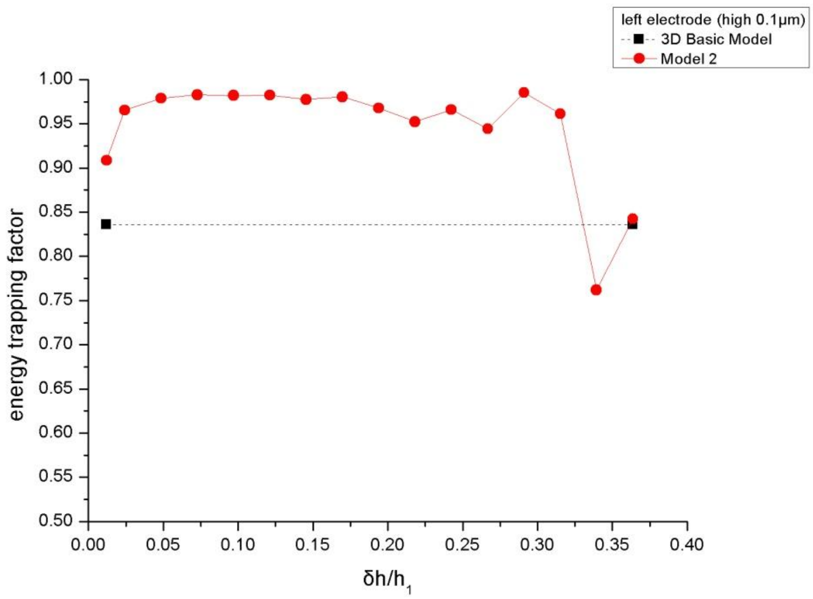

Fig 4. 13 Energy Trapping Curve of Model 2 Left Electrode

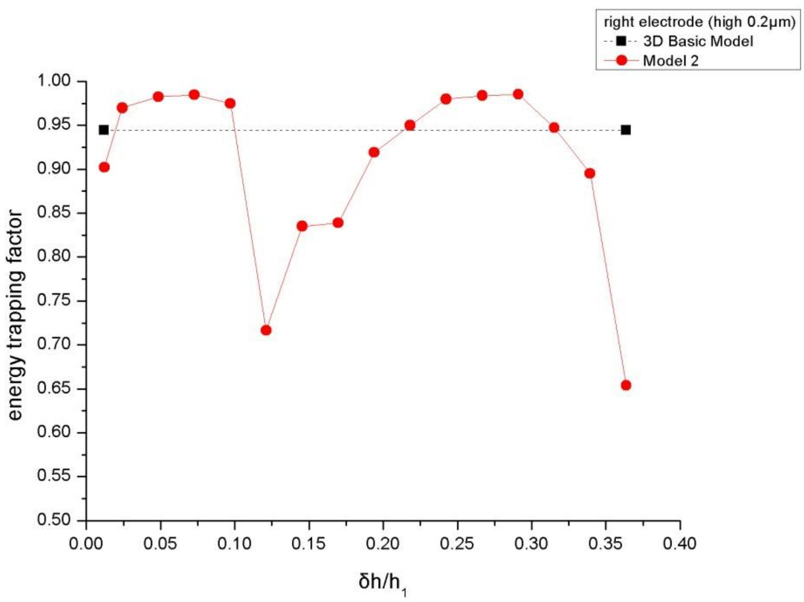

Fig 4. 14 Energy Trapping Curve of Model 2 Right Electrode

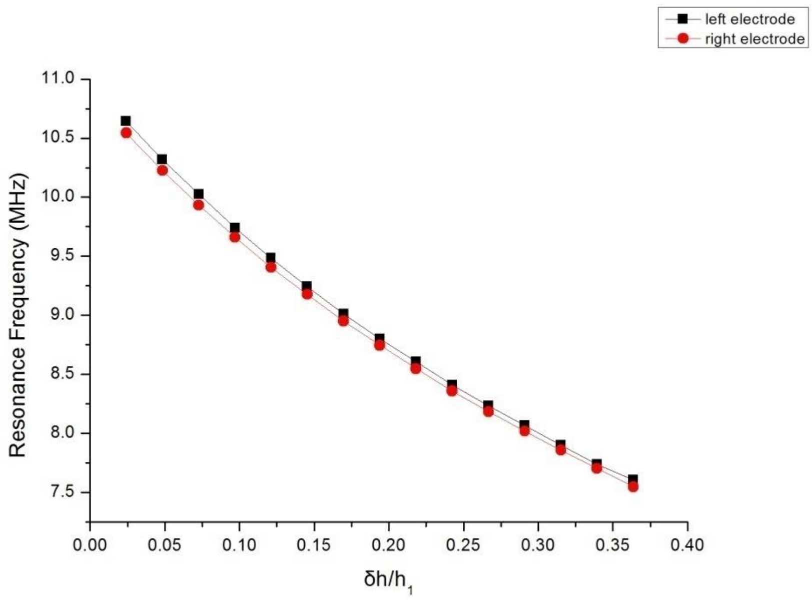

Fig 4. 15 Resonance Frequency of Model 2

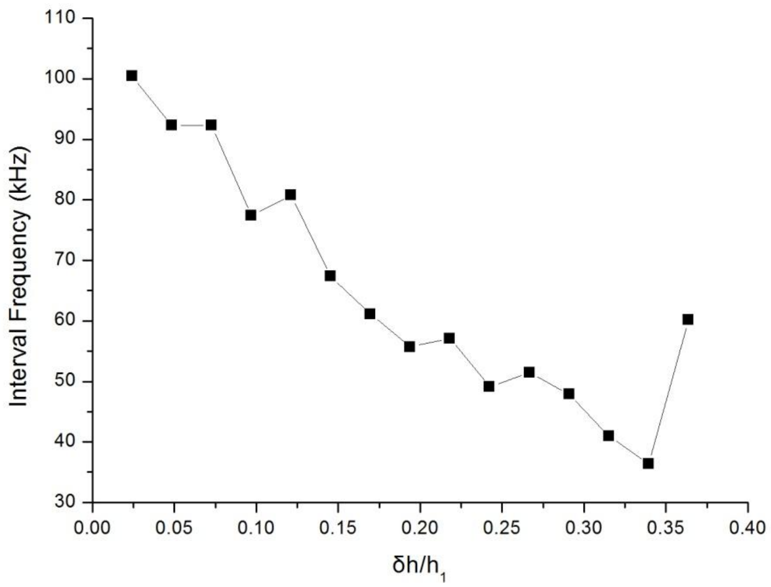

Fig 4. 16 Interval Frequency of Model 2

4.3.3 Three-dimensional Mesa Design –Model 3

As shown in Fig 4.17 and 4.18, model 3 is the sketch stretching the two-dimensional mesa design along the z-direction directly. However, the dimension of electrode except the height of mesa stays unchangeable as the three-dimensional basic model. And the simulation results are shown below.

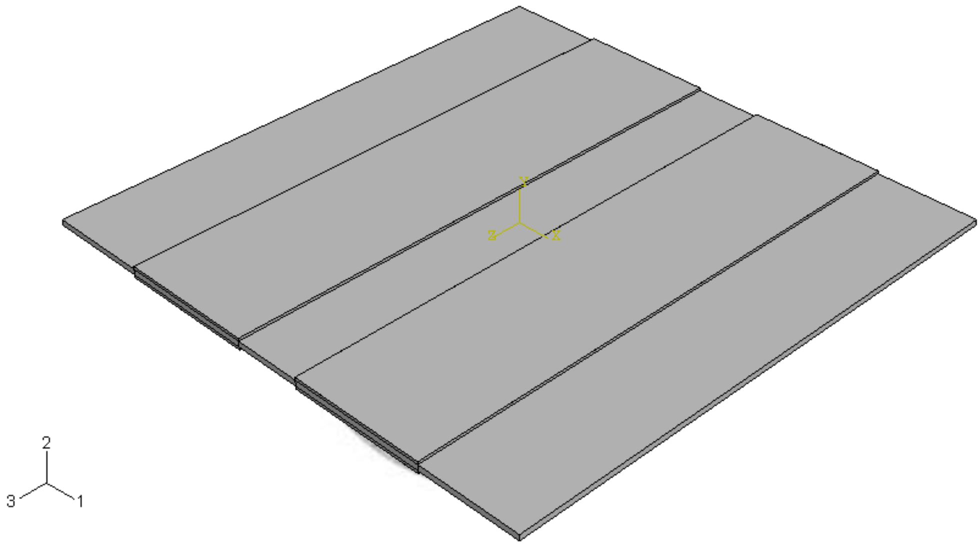

Fig 4. 17 Sketch of Model 3

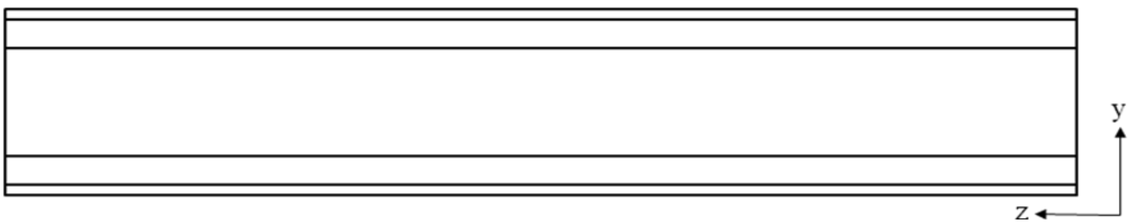

Fig 4. 18 YZ-plane Sketch of Model 3

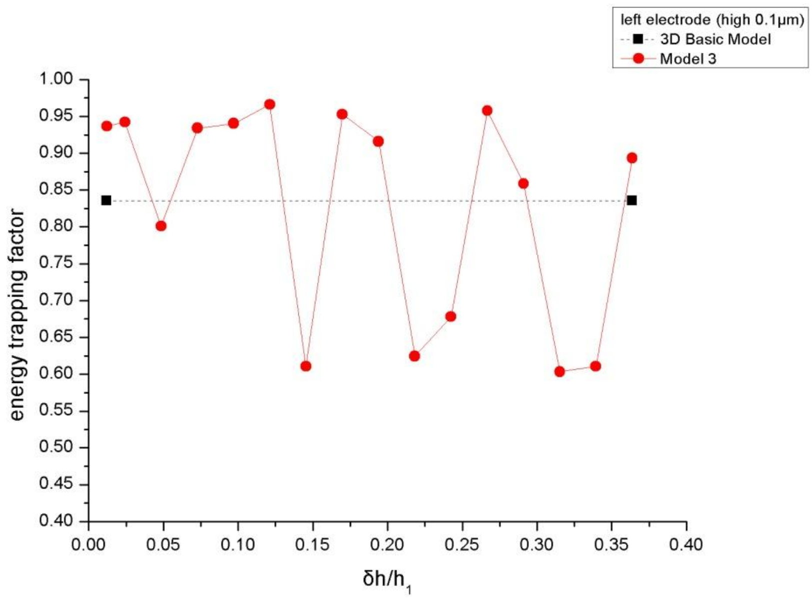

Fig 4. 19 Energy Trapping Curve of Model 3 Left Electrode

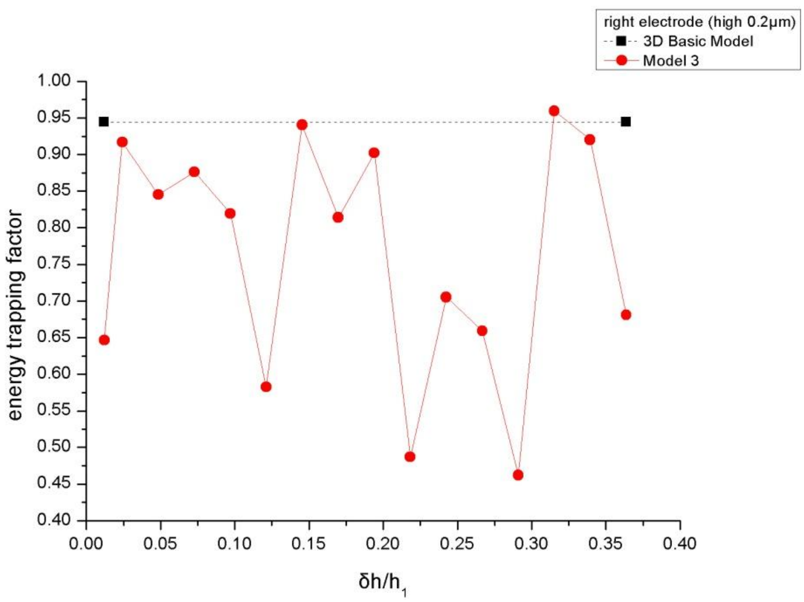

Fig 4. 20 Energy Trapping Curve of Model 3 Right Electrode

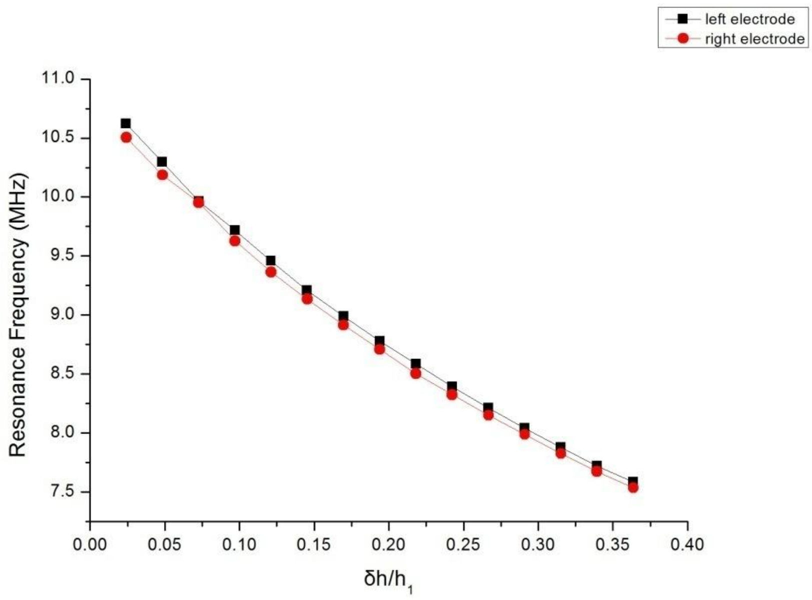

Fig 4. 21 Resonance Frequency of Model 3

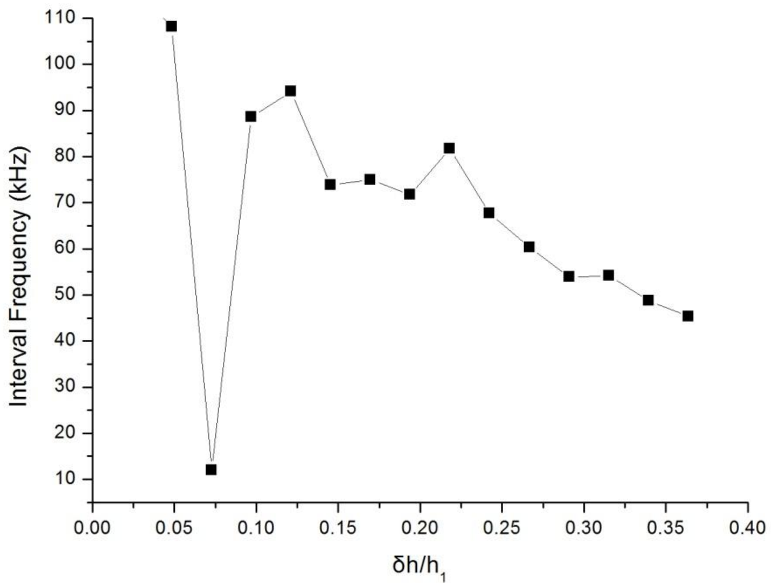

Fig 4. 22 Interval Frequency of Model 3

4.3.4 Investigation of Mesa Design Model

Refer to the previous simulation results, the energy trapping effect of model 3 is inferior to that of model 1 and model 2. The frequency of drop point in model 3 appears too often to be an ideal pattern. In the right electrode, it shows better performance on three-dimensional basic model than most dimensions in the mesa design of model 3. For the reasons above, model 3 is not appropriate to be an example while designing. The following figures are the comparisons between model 1 and 2 for both contain similar energy trapping effect.

There is something in common about the curves shown in Fig 4.23 and Fig 4.24. In left electrode, the energy trapping effect decreases when $\delta h > 28mm$ and model 2 compared to model 1 is apparently stable to dramatically restrict the incidence of drop point. In right electrode, the drop point for both models occurs obviously in the neighborhood of $\delta h = 10mm$ and the energy trapping effect turns to diminish as $\delta h > 26mm$.

Roughly speaking, the frequency drift of three models gets less linearly with the raise of mesa height. As for the interval frequency, it is greater than 35kHz and reduces with the increase of mesa height.

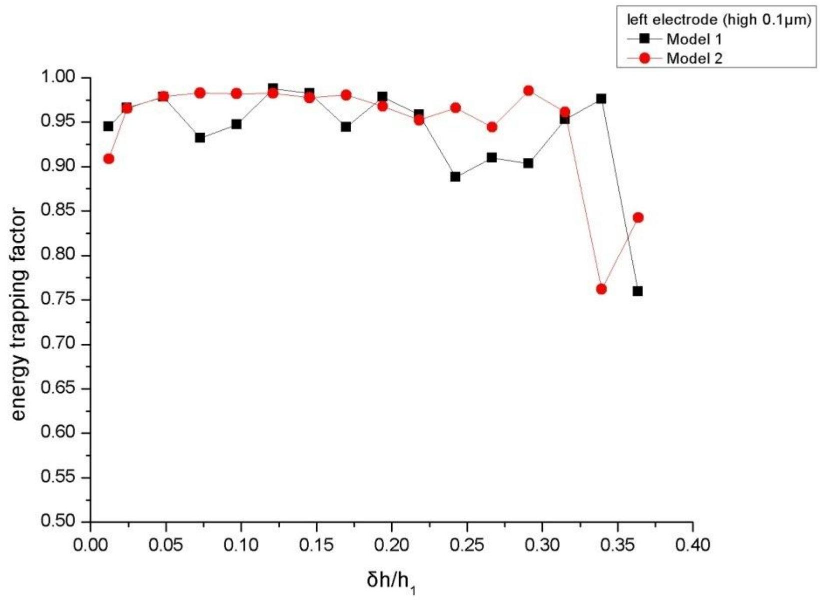

Fig 4. 23 Energy Trapping Curve for Left Electrode of Model 1and Model 2

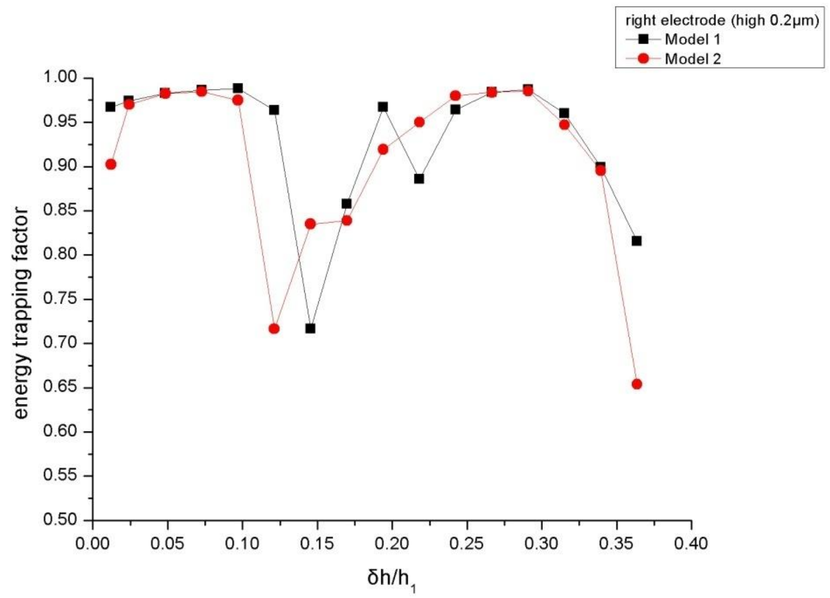

Fig 4. 24 Energy Trapping Curve for Right Electrode of Model 1and Model 2

4.4 Three-dimensional Bi-step Design

In 2002, Goka et al [16] brought up an idea of bi-step mesa design and verified that it enhanced the decoupling characteristics between thickness-share wave and spurious wave more efficiently than mesa design. In 2005, Lu et al [18] further confirmed its better efficacy through computing the value of energy trapping effect. The XY-plane sketch of bi-step design is shown below.

L is the length of the quartz crystal and a is the width of electrode. b is the distance from the quartz center to the electrode while c is from the quartz boundary to the electrode. h_1 is the height of the quartz and h_{e1} and h_{e2} stand for the height of left and right electrode each. H_1, H_2, L_1 and L_2 are the dimensions of bi-step mesa design and the sum of H_1 and H_2 equals the mesa height. Here, we extend the two-dimensional model to the three-dimensional one in light of the same technique with the previous chapter and then develop three different shapes below.

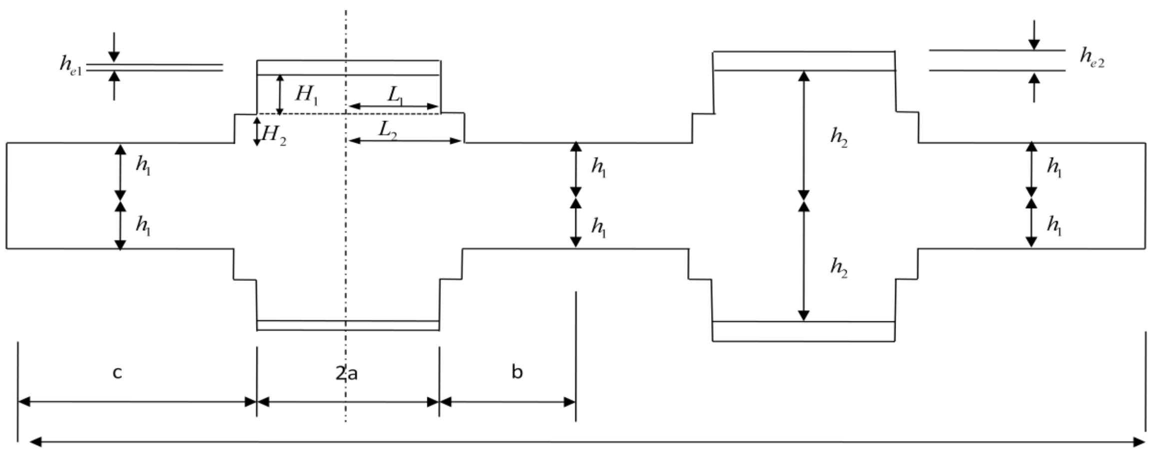

Fig 4. 25 The XY-plane Sketch of Bi-step Design

4.4.1 Three-dimensional Bi-step Design -Model 4

Model 4 is a familiar sketch of bi-step design today. The conception is to load another quartz mesa on the primary mesa structure, and under the prerequisite of fixed electrode size, we widen L_2 and modify the variables H_1 and H_2 to accomplish our purpose ameliorating energy trapping effect. The dimension chosen here is consistent with the three-dimensional basic model exclusive of L_2, H_1 and H_2.

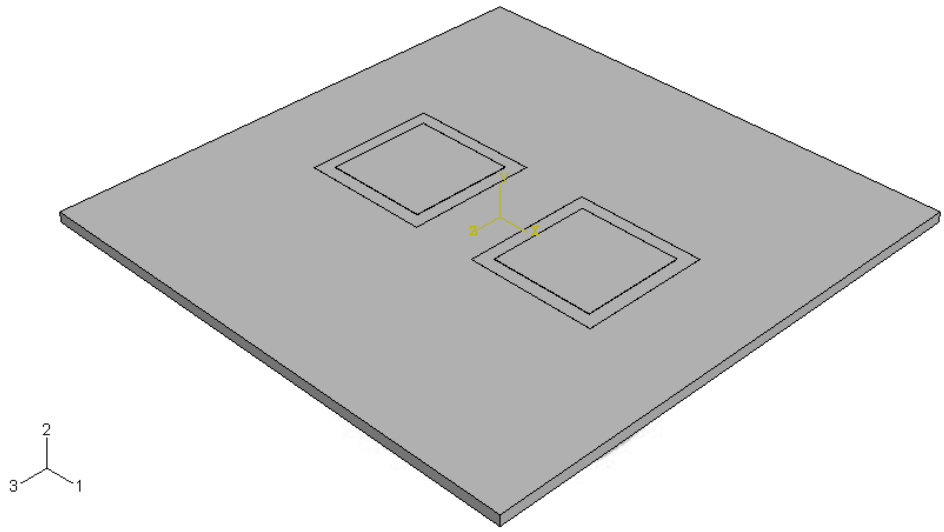

Fig 4. 26 Sketch of Model 4

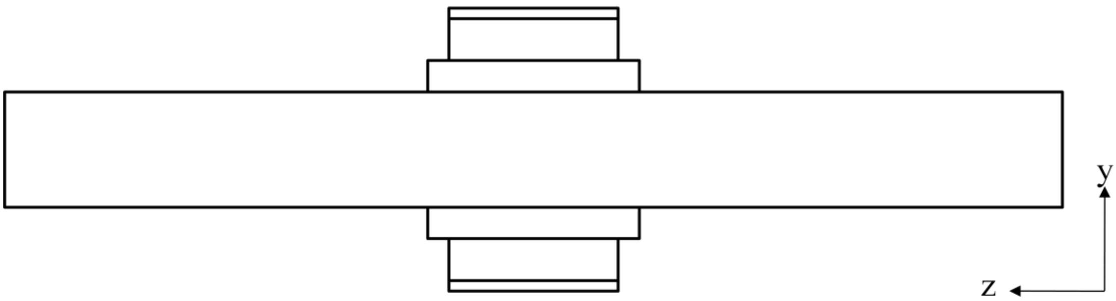

Fig 4. 27 YZ-plane Sketch of Model 4

4.4.2 Three-dimensional Bi-step Design -Model 5

Fig 4.28 and 4.29 illustrate the sketch of model 5, which is constructed out of stretching the second step (H_2 and L_2) along the z-direction and keeping the first step (H_1 and L_1) and electrodes as a shape of square. Instead of L_2, H_1 and H_2, model 5 and the three-dimensional basic model possess the coherent dimension.

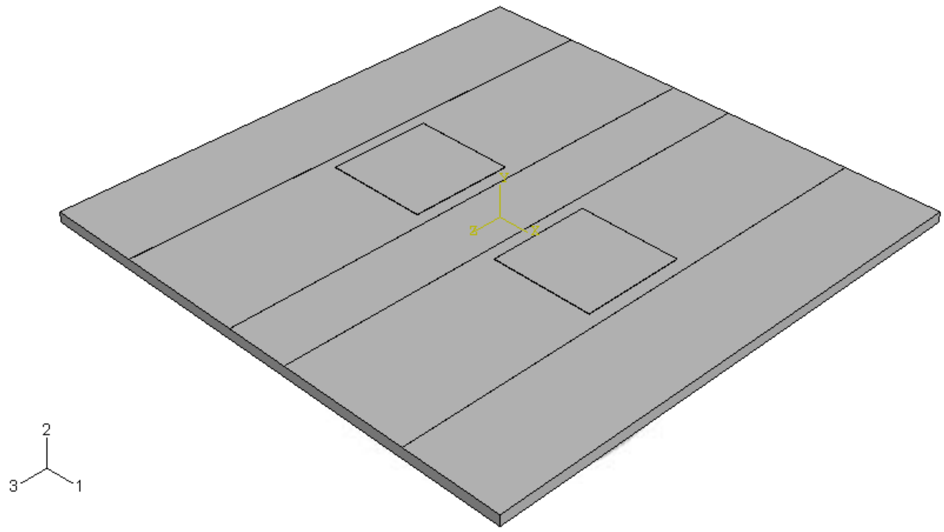

Fig 4. 28 Sketch of Model 5

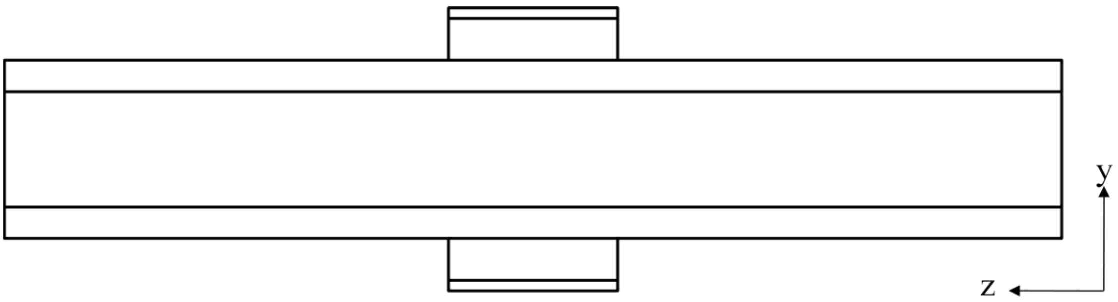

Fig 4. 29 YZ-plane Sketch of Model 5

4.4.3 Three-dimensional Bi-step Design -Model 6

As shown in Fig 4.30 and 4.31, model 6 is the sketch extending the quartz in two-dimensional bi-step design along the z-direction and keeping the electrode as a shape of square. Like model 4 and 5, the dimension chosen here is correspondent with the three-dimensional basic model except L_2, H_1 and H_2.

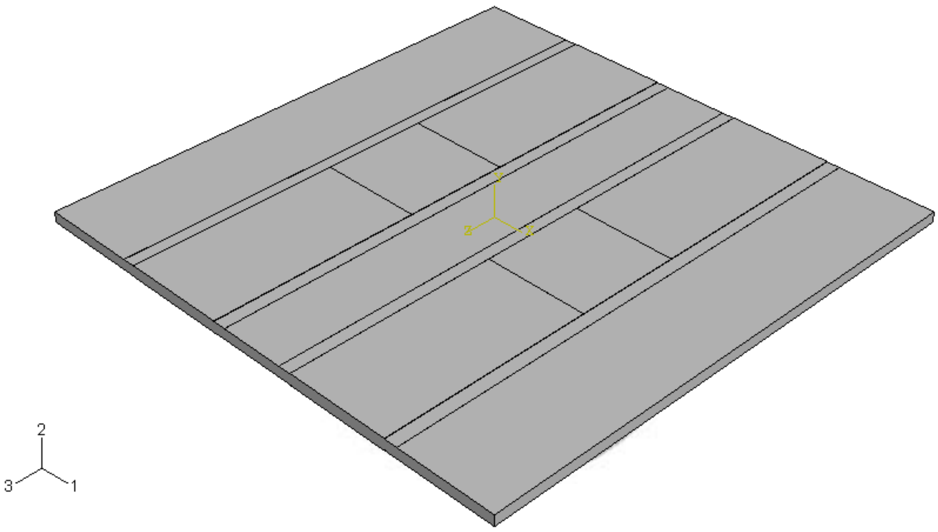

Fig 4. 30 Sketch of Model 6

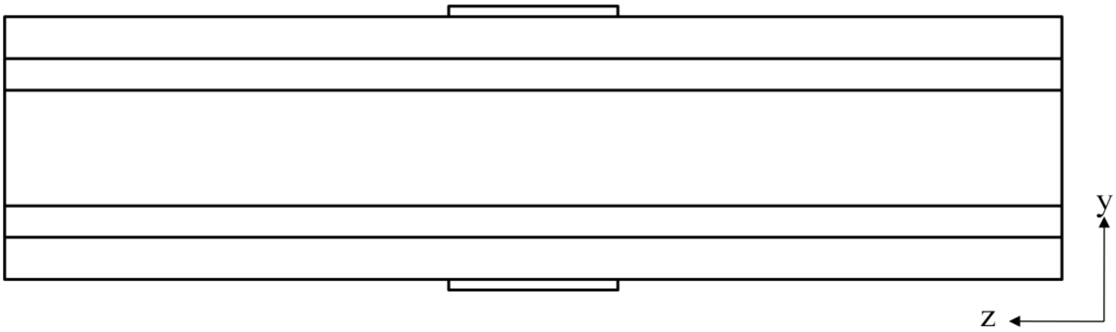

Fig 4. 31 YZ-plane Sketch of Model 6

4.4.4 Bi-step Design Simulation Result of Variable L_2

Because of several variables in bi-step design, it is necessary to examine the sensitivity of each variable. First of all, we fix the mesa height and define $\delta h=H_1+H_2$. Meanwhile, the two steps are with the same height (H1=H2=1/2δh). In order to progress the performance of the drop point, the size leading to the worst situation in Fig 4.23 and Fig 4.24 is studied (δh=12mm). We try to come up with the perfect dimension of the variable L_2 via energy trapping effect.

From the Fig 4.32 and Fig 4.33, the value of L_2 does not have enormous influence on model 4 and model 6. Considering model 4 to 6 at the same time, the value of L_2 is recommended to 1.3 mm. Afterward, the step height is the next issue.

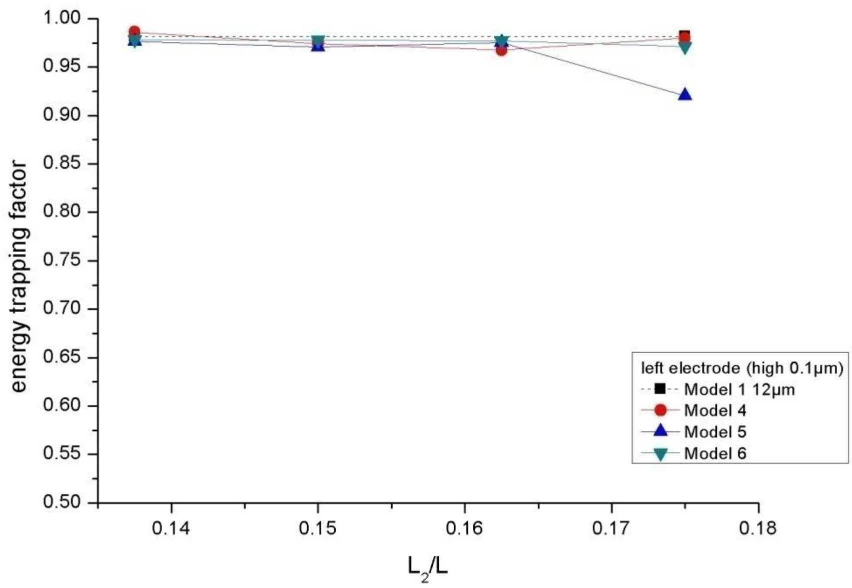

Fig 4. 32 Energy trapping factor curve with the Valiable L_2 for Left Electrode

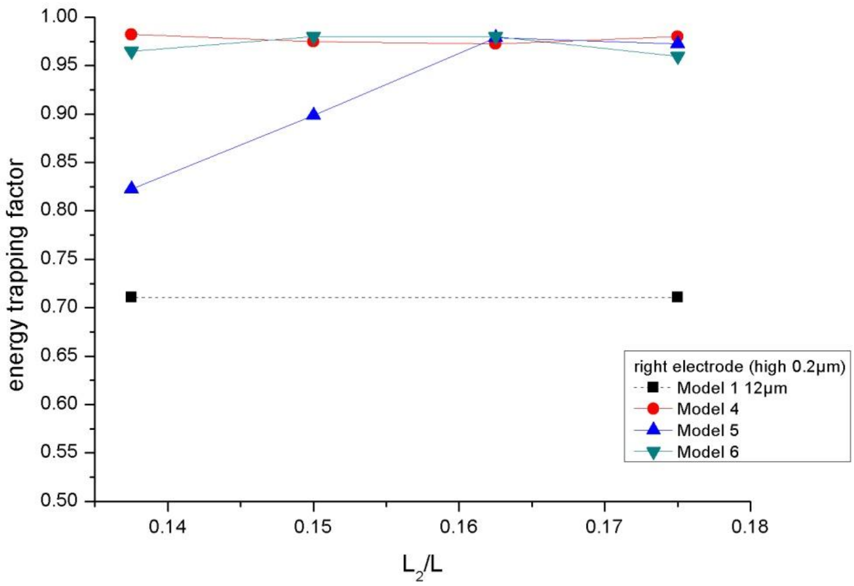

Fig 4. 33 Energy trapping factor curve with the Valiable L_2 for Right Electrode

4.4.5 Bi-step Design Simulation -(1)

In the beginning, we adjust the total mesa height to $\delta h=H_1+H_2=12\mu m$ and then take H_1 as an independent variable. And the simulation results are shown below.

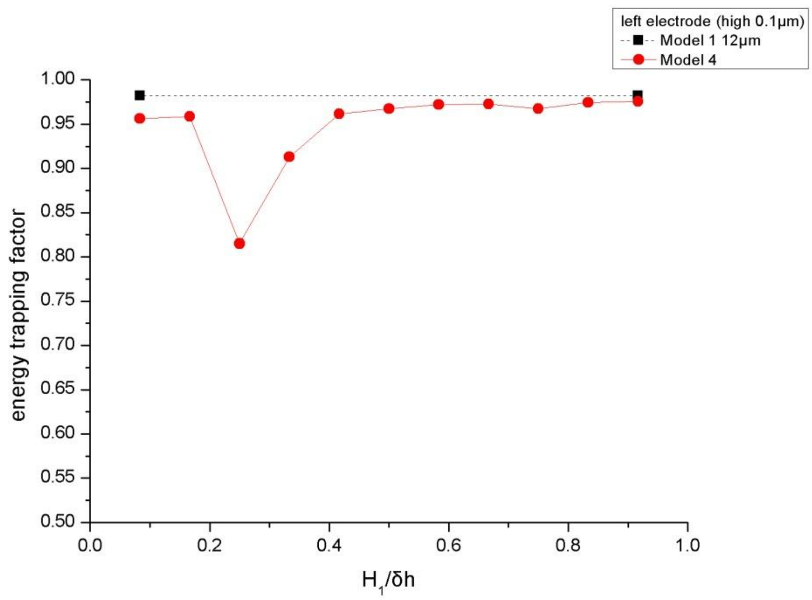

Fig 4. 34 Energy Trapping Curve of Model 4 Left Electrode in Simulation (1)

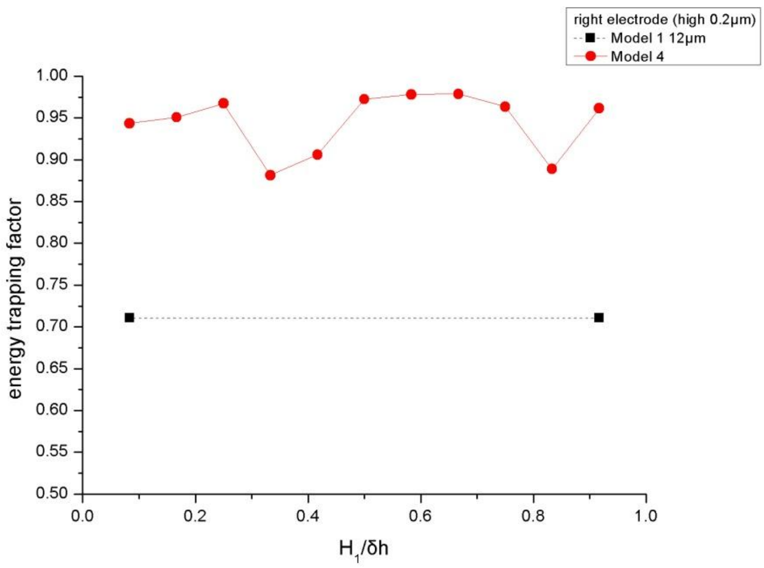

Fig 4. 35 Energy Trapping Curve of Model 4 Right Electrode in Simulation (1)

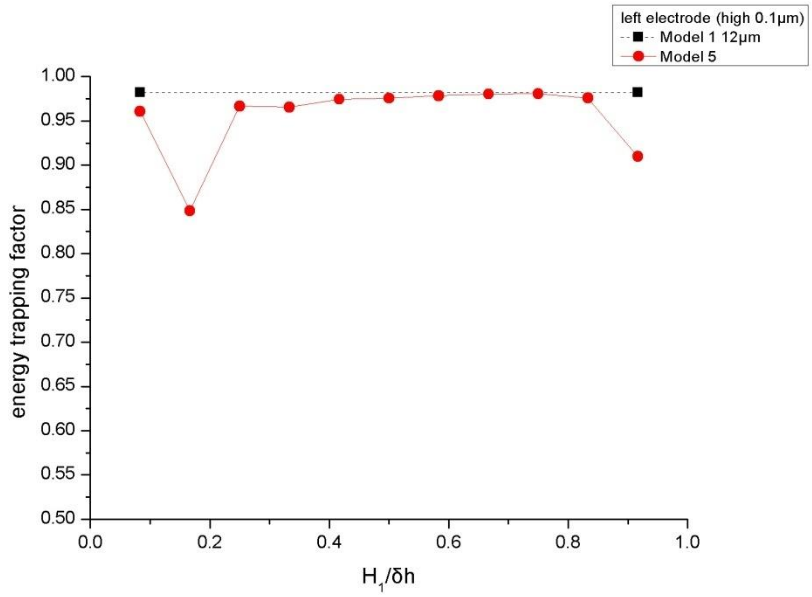

Fig 4. 36 Energy Trapping Curve of Model 5 Left Electrode in Simulation (1)

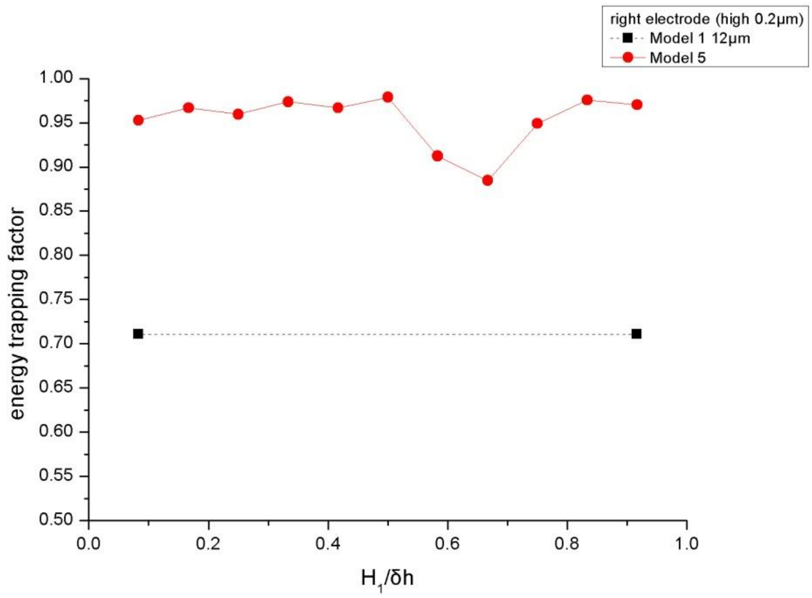

Fig 4. 37 Energy Trapping Curve of Model 5 Right Electrode in Simulation (1)

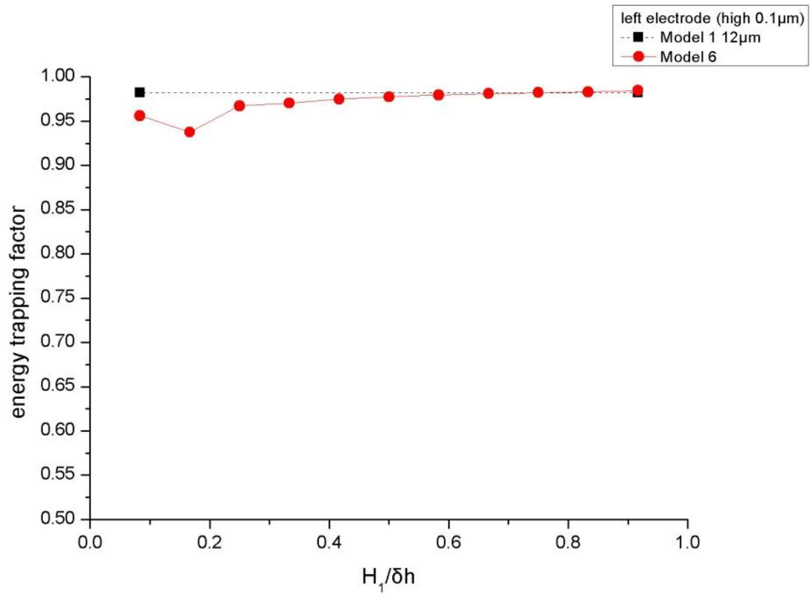

Fig 4. 38 Energy Trapping Curve of Model 6 Left Electrode in Simulation (1)

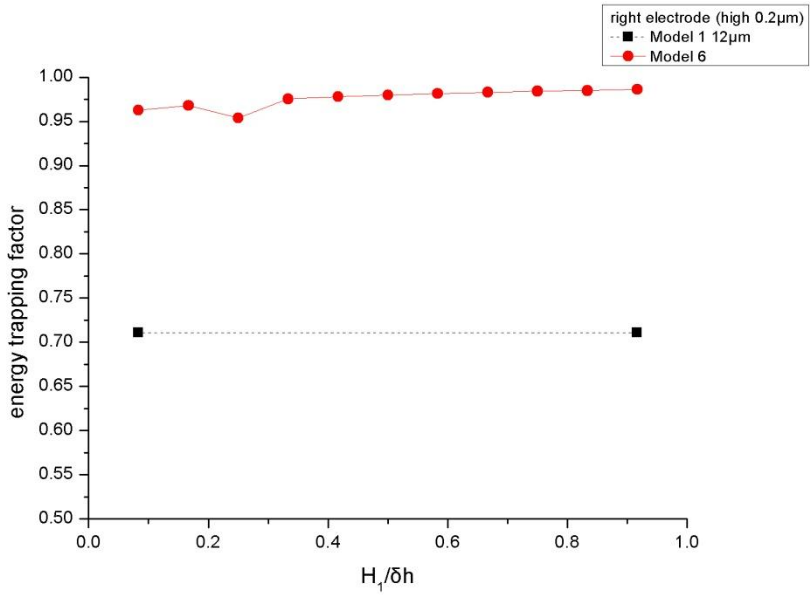

Fig 4. 39 Energy Trapping Curve of Model 6 Right Electrode in Simulation (1)

4.4.6 Bi-step Design Simulation -(2)

The value of mesa height which results in the best performnace of energy trapping effect in Fig 4.23 and Fig 4.24 (δ h=8μ m) is practiced. In addition, we assume the total mesa height toδ h=H_1+H_2=8μ m and execute the same technique with the simulation (1) that is L2=1.3mm and H_1 is an independent variable.

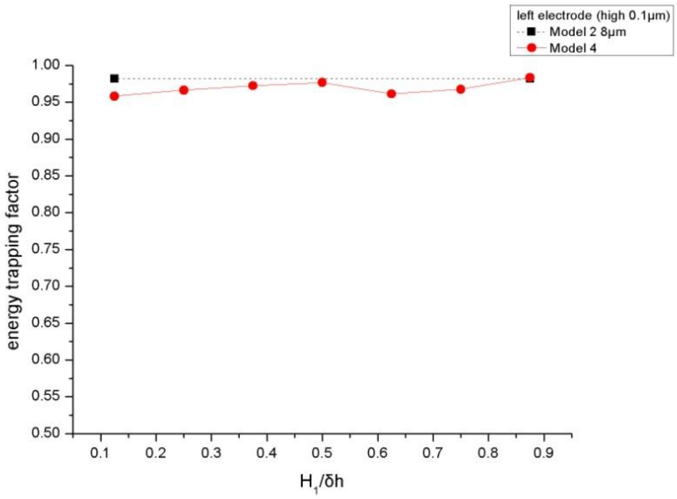

Fig 4. 40 Energy Trapping Curve of Model 4 Right Electrode in Simulation (2)

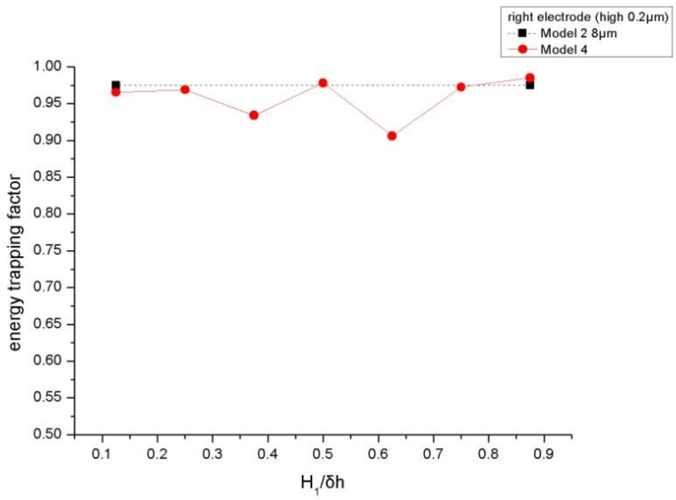

Fig 4. 41 Energy Trapping Curve of Model 4 Right Electrode in Simulation (2)

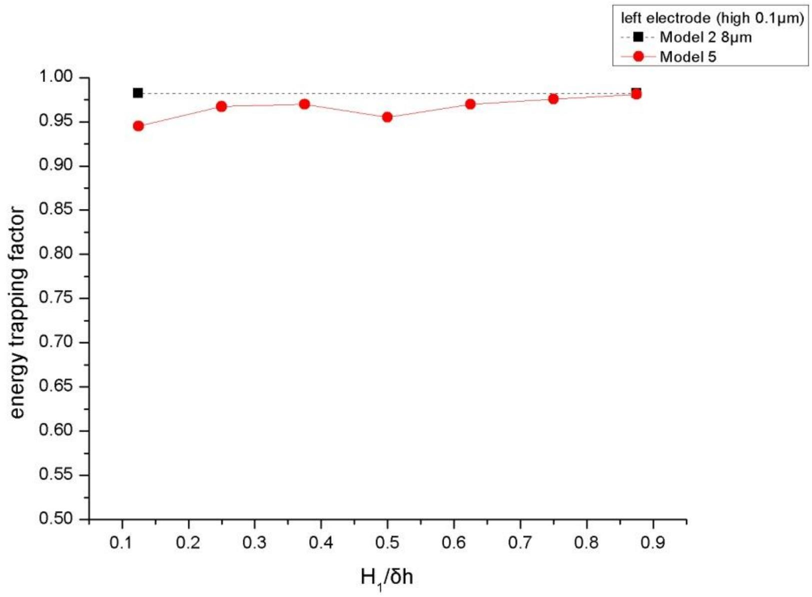

Fig 4. 42 Energy Trapping Curve of Model 5 Left Electrode in Simulation (2)

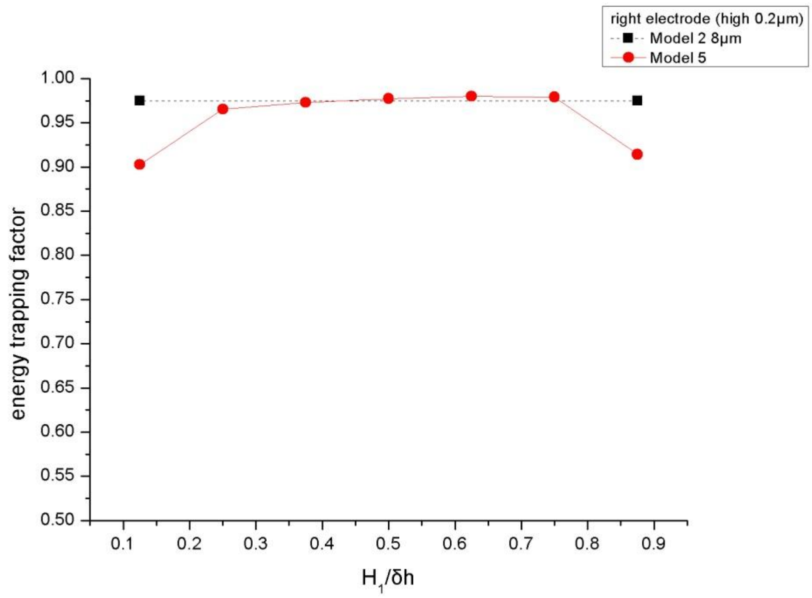

Fig 4. 43 Energy Ttrapping Curve of Model 5 Right Electrode in Simulation (2)

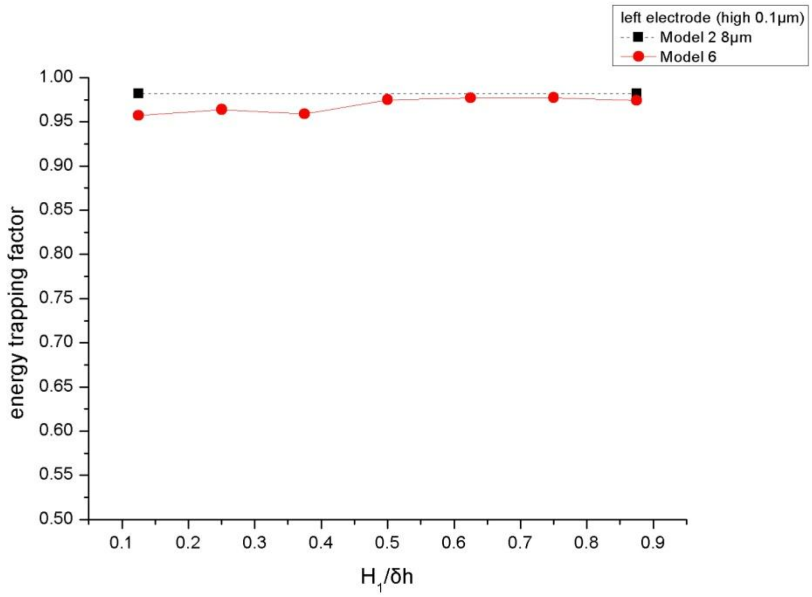

Fig 4. 44 Energy Trapping Curve of Model 6 Left Electrode in Simulation (2)

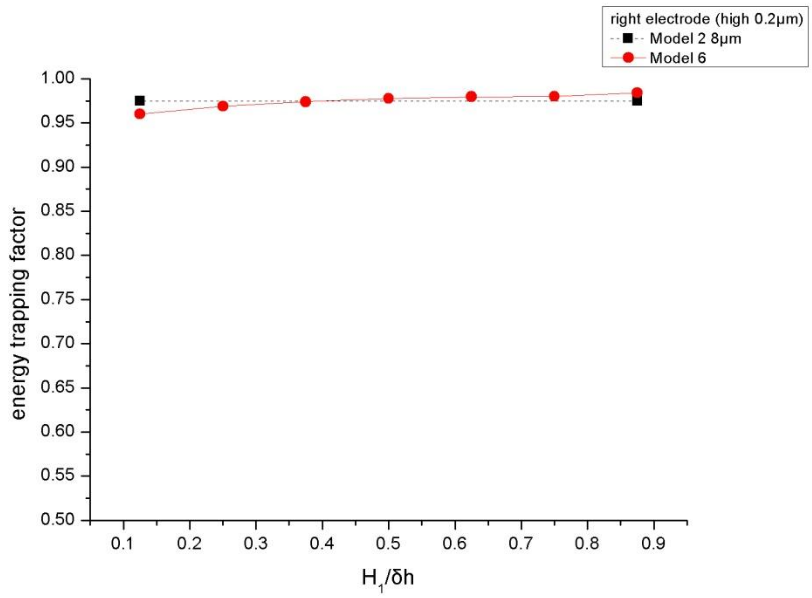

Fig 4. 45 Energy Trapping Curve of Model 6 Right Electrode in Simulation (2)

4.4.7 Investigation of Bi-step Design Simulation

According to the simulation result (1), the three models of bi-step all amend their performance effectively. However, the occurrence of drop point still exists in model 4 and model 5. In the result (2), although the value of energy trapping effect does not transcend the chosen size in mesa design, the performance is acceptable. Besides, there is something interesting found in result (1) and (2). The effect of model 6 displays nearly linear increasing phenomenon and the maximum is achieved at the end of the curve which means H_2=1μ m. This trend is constructive to the optimal model. .

4.4.8 Bi-step Design Simulation -(3)

Simulation (3) takes advantage of the trend of model 6 to carry out the fittest model. For this simulation, model 2 and model 6 are compared in the same mesa height and the dimension of model 6 has been ascertained as follows: L2=1.3mm, H_2=1μ m. From the results, the curve of bi-step is smooth and with unapparent drop points. Furthermore, the value is greater than 90 for all points in the curve. The frequency drift of model 6 gets less linearly with the raise of first step height. As for the interval frequency, it is greater than 35,000Hz and reduces with the increase of first step height. This phenomenon has the same trend with mesa design.

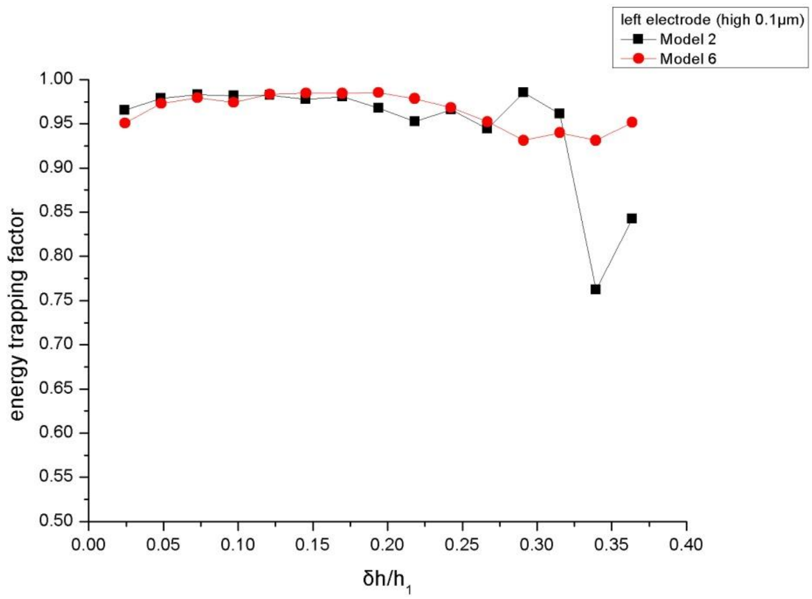

Fig 4. 46 Energy Trapping Curve of Left Electrode in Model 2 and Model 6 with The Same Height

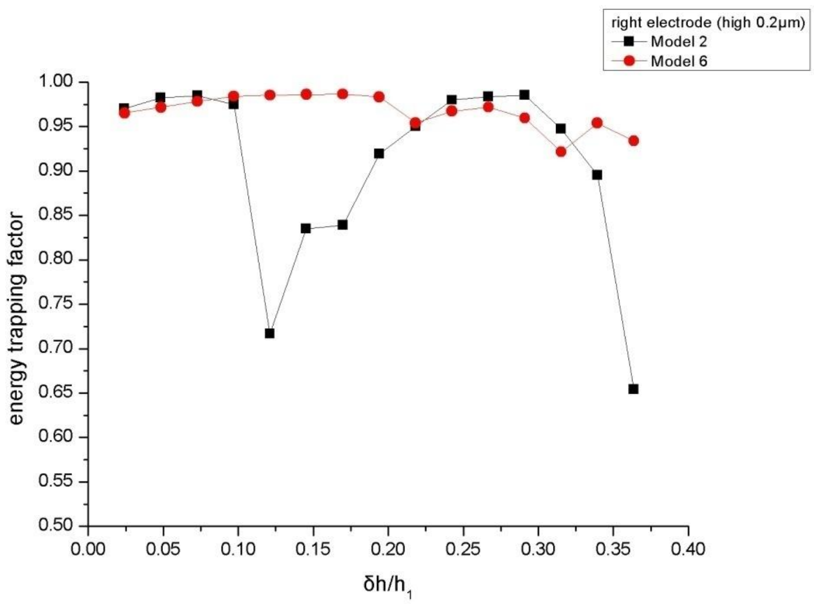

Fig 4. 47 Energy Tapping Curve of Right Electrode in Model 2 and Model 6 with The Same Height

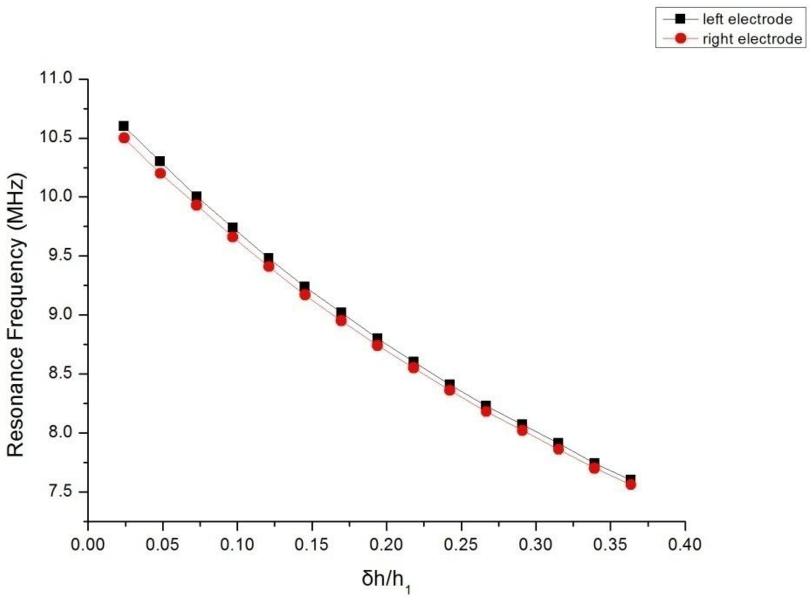

Fig 4. 48 Resonance Frequency of Model 6 (L_1=1mm L_2=1.3mm, H_2=1μm)

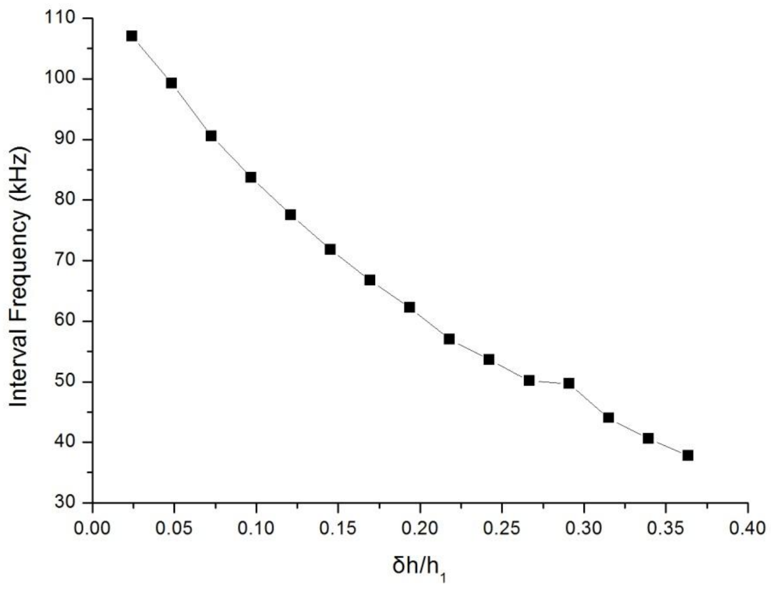

Fig 4. 49 Interval Frequency of Model 6 (L_1=1mm L_2=1.3mm, H_2=1μm)

Chapter 5 Conclusion and Future Work

5.1 Conclusion

In this thesis, finite element analysis software is utilized to simulate the dual-channel QCM. The three-dimensional basic model of dual-electrode QCM is produced by extending from the two-dimensional basic model. And to improve the accuracy of our measurement, the mesa design is introduced. However, there are disadvantages to the mesa design, for example the occurrence of dropping points. To overcome the drawback, the bi-step design is recommended and it can further help accomplish one of the purposes of this research—the miniaturization of dual-channel QCM. Based on the simulation, we can conclude that:

1. At some specific mesa heights ($2\mu m<\delta h<8\mu m$, $20\mu m<\delta h<26\mu m$), the mesa design can improve QCM accuracy by increasing energy trapping effect.
2. The dropping points take place unpredictably in mesa design. And when the mesa height reaches to greater than $28\mu m$, that's to say it exceeds 34% of the plate thickness, the effect will be reduced obviously.
3. In mesa design, the model 2 gives superior performance.

4. The bi-step design can improve the situation where the dropping points occur in some mesa design sizes.
5. In bi-step design, model 6 gives superior performance when it is set to L2=1.3mm H2=1μm.
6. In model 6, H_1 is recommended to be ranged in the size between 1μm to 15μm, H_2 equals 1μm, and L_2 equals 1.3mm.

5.2 Future Work

In this thesis, the three-dimensional simulation research results are not compared with other reliable statistics because to date, there is still no analytical approach to three-dimensional piezoelectric plate. And since the QCM is measured in the liquid phase in its operation, the force between liquid and the piezoelectric plate will extend influence over resonance frequency. As a result, if we can take all these factors which are noted above into consideration, this simulation will be more complete and accurate.

Reference

[1] Curie, J., Curie, P., Development by pressure of polar electricity in crysatals with angled face, *Comput. Rend. Acad. Sci. Paris,* (1880), pp. 294-297

[2] Rayleigh, *L.*, On the free vibrations of an infinite plate of homogeneous isotropic elastic matter, *proc. Lond. Math Soc.*, (1889), Vol. 20, pp. 225-226

[3] Cady, W. G., Crystal physics of interaction process, *Phys*, (1959), 155,206-222

[4] Lack, F. R., Willard, G. W., Some improvements in quartz crystal circuit elements, *Bell Syst. Technol.*, (1934), Vol. 13, pp. 453-455

[5] Mindlin R. D., Thickness-shear and flexural vibrations of crystal plates, *J. Appl. Phys.*, (1951), Vol. 22, No.3, pp. 316-323

[6] Sauerbray, Use of quartz crystal vibrator for weighting thin films on a microbalance, *G.Z.Phys.*,(1959), Vol.155, pp. 206-222.

[7] Mindlin, R. D., Lee P. C. Y., Thickness-shear and flexural vibration of partially plate crystal plate crystal plates, *Int, J. Solid Struct.*, (1965), Vol. 2, pp. 125-139

[8] J. L. Bleustein and H. F. Tiersten, Forced thickness-shear vibrations of discontinuously plated piezoelectric plates, *J. Acoust. Soc. Amer*, (1968), Vol. 43, pp. 1311–1318,

[9] Nomura, T., Okuhara, Influence of roughness on the admittance of the quartz

crystal microbalance immersed in liquids, M., *Anal. Chem. Acta*, (1982), Vol. 142, pp. 281-284

[10] Kurosawa, S., Tawara, E., Kamo, N., Kobataka, Oscillating frequency of piezoelectric quartz crystal in solutions, Y., *Anal. Chem. Acta*, (1990), Vol. 230, pp. 41-49

[11] K. Hirama and Y. Aoyama, Energy trapping behavior of AT-Cut quartz crystal resonators with a groove ring on main electrodes, *Electronics and Communications*,(1999), Vol. 82, pp. 48-55

[12] K. Hirama, Y. Aoyama, R. Yasuike and K. Y. Amazaki, Trapped-energy AT-CUT quartz crystal units with grooves, *IEEE International Frequency Control Symposium*,(1997), pp. 750-757

[13] Tatsuma, T., Watanabe, Y., Oyama, N., Kitakizaki, K., Haba, M., Multichannel quartz crystal mcrobalance, *Anal. Chem. Acta*,(2001), Vol. 71, pp. 3632-3636

[14] A. Ishizaki, H. Sekimoto, D. Tajima and Y. Watanabe, Analysis of spurious vibrations in mesa-shaped AT-cut quartz plates, *IEEE Ultrasonics Symposium* (1995), pp. 913-916

[15] Ishizaki Akio, Grooved AT-CUT quartz plate, *IEEE/EIA International Frequency Control Symposium and Exhibition*, (2000), pp. 416-419

[16] S. Goka, H. Sekimoto, Y. Wantanabe, T. Sato and K. Sato, Mode decoupling effect of multi-stepped bi-mesa AT-cut quartz resonator, *IEEE International Frequency Control Symposium and PDA Exhibition*, (2003), pp. 694-697

[17] F. Lu, H. P. Lee, P Lu and S. P. Lim, Finite Element Analysis of interference for the laterally coupled quartz crystal microbalances, *Sensor &Actuators*, (2005), Vol. 119, pp. 90-99

[18] F Lu, H P Lee and S P Lim, Energy-trapping analysis for the bi-stepped mesa quartz crystal microbalance using the finite element method, *Smart Materials and Structures*, (2005), Vol. 14, pp. 272–280

[19] F. Shen and P. Lu, Influence of interchannel spacing on the dynamical properties of multichannel quartz crystal microbalance, *IEEE Transactions on Ultrasonics*, (2004), Vol. 51, pp. 249-253

[20] O'Shea, K. H. Lee, P. Lu and T. Y. Ng, Frequency interference between two mesa-shaped quartz crystal microbalances, *IEEE Transactions on Ultrasonics, Ferroelectrics, and Frequency Control,* (2003), Vol. 50, pp. 668-675

[21] F. Shen, P. Lu, S. J. O'Shen and K. H. Lee, Frequency coupling and energy trapping in mesa-shaped multi-channel quartz crystal microbalances, *SENSOR& Actuators*, (2004), Vol. 111, pp. 180-187

[22] S. Pantalei, E. Zampetti, A. Macagnano, A. Bearzotti, I. Venditti and M. V.

Russo, Enhanced sensory properties of a multichannel quartz crystal, *Sensors* (2007),Vol. 7, pp. 2920-2928

[23] W. Shockley, C. Corporation, P. Alto, D. R. Curran and D. J. Koneval, Energy trapping and related studies of multiple electrode filter crystals, *Annual Symposium on Frequency Contro* , (1963**)**, pp. 88- 126

Appendix-Material constant

AT-cut quartz

Density: $\rho_q = 2675[kg/m^3]$

Anisotropic elastic coefficient constant matrix:

$$C = \begin{bmatrix} 86.74 & -8.25 & 27.15 & -3.66 & 0 & 0 \\ -8.25 & 129.77 & -7.42 & 5.7 & 0 & 0 \\ 27.15 & -7.42 & 102.83 & 9.92 & 0 & 0 \\ -3.66 & 5.7 & 9.92 & 38.61 & 0 & 0 \\ 0 & 0 & 0 & 0 & 68.81 & 2.53 \\ 0 & 0 & 0 & 0 & 2.53 & 29.01 \end{bmatrix} \times 10^9 \left[N/m^2\right]$$

Piezoelectric constant matrix:

$$e = \begin{bmatrix} -0.171 & 0.152 & 0.0187 & -0.067 & 0 & 0 \\ 0 & 0 & 0 & 0 & -0.108 & 0.095 \\ 0 & 0 & 0 & 0 & 2.53 & 29.01 \end{bmatrix} \left[C/m^2\right]$$

Dielectric constant matrix:

$$\varepsilon = \begin{bmatrix} 39.21 & 0 & 0 \\ 0 & 39.82 & 0.86 \\ 0 & 0.86 & 40.42 \end{bmatrix} \times 10^{-12} \left[C/Vm\right]$$

Gold

Density: $\rho_g = 18500[kg/m^3]$

Young’s modules: 95.05[GPa]

Poison ratio: 0.42